Molecular Pharmacology Fast Forward. Published on June 12, 2018 as DOI: 10.1124/mol.118.112359
This article has not been copyedited and formatted. The final version may differ from this version.

Discovery, characterization, and effects on renal fluid and electrolyte excretion of the Kir4.1 potassium channel pore blocker, VU0134992

Sujay V. Kharade, Haruto Kurata, Aaron M. Bender, Anna L. Blobaum, Eric Figueroa, Amanda Duran, Meghan Kramer, Emily Days, Paige Vinson, Daniel Flores, Lisa M. Satlin, Jens Meiler, C. David Weaver, Craig W. Lindsley, Corey R. Hopkins, and Jerod S. Denton

Department of Anesthesiology, Vanderbilt University Medical Center, Nashville, TN 37232: SVK, MK, JSD
Center for Neuroscience Drug Discovery and the Vanderbilt Specialized Chemistry Center for Accelerated Probe Development, Vanderbilt University, Nashville, TN 37232: KH, AMB, ALB, CWL, CRH
Department of Pharmacology, Vanderbilt University, Nashville, TN 37232: HK, AMB, EF, JM, CDW, CWL, JSD
Department of Chemistry, Vanderbilt University, Nashville, TN 37232: AD, JM, CDW, CWL
High-Throughput Screening Center, Vanderbilt University, Nashville, TN 37232: ED, PV
Department of Pediatrics, Icahn School of Medicine at Mount Sinai, New York, New York, 10029: DF, LMS
Department of Pharmaceutical Sciences, University of Nebraska Medical Center, Omaha, NE 68198-6125: CRH
Institute of Chemical Biology, Vanderbilt University, Nashville, TN 37232: CDW, CWL, JSD

Molecular Pharmacology Fast Forward. Published on June 12, 2018 as DOI: 10.1124/mol.118.112359
This article has not been copyedited and formatted. The final version may differ from this version.

Running Title: Kir4.1 inhibitor: VU0134992

Number of text pages: 19
Number of tables: 2
Number of figures: 6
Number of references: 61
Number of words in Abstract: 298
Number of words in Introduction: 757
Number of words in Discussion: 1,779

Corresponding authors:
Jerod S. Denton, Ph.D.
T4208 Medical Center North
1161 21st Avenue South
Nashville, TN 37232
jerod.s.denton@vanderbilt.edu

Corey Hopkins, Ph.D.
Department of Pharmaceutical Sciences
College of Pharmacy
University of Nebraska Medical Center
986125 Nebraska Medical Center
Omaha, NE 68198-6125
corey.hopkins@unmc.edu

Abbreviations: CCD, cortical collecting duct; DCT, distal convoluted tubule; EAST, Epilepsy Ataxia Sensorineural deafness Tubulopathy; MECP2, methyl CpG binding protein 2; SIDS, sudden infant death syndrome; TAL, thick ascending loop; SeSAME, Seizures Sensorineural deafness Mental retardation Electrolyte imbalances; SSRI, Selective Serotonin Reuptake Inhibitor; TCA, tricyclic antidepressant; VU0134992, 2-(2-Bromo-4-iso-propylphenoxy)-*N*-(2,2,6,6-tetramethylpiperidin-4-yl)acetamide

Molecular Pharmacology Fast Forward. Published on June 12, 2018 as DOI: 10.1124/mol.118.112359
This article has not been copyedited and formatted. The final version may differ from this version.

ABSTRACT

The inward rectifier potassium (Kir) channel Kir4.1 (*KCNJ10*) carries out important physiological roles in epithelial cells of the kidney, astrocytes in the central nervous system, and stria vascularis of the inner ear. Loss-of-function mutations in *KCNJ10* lead to EAST/SeSAME syndrome, which is characterized by epilepsy, ataxia, renal salt wasting, and sensorineural deafness. While genetic approaches have been indispensable for establishing the importance of Kir4.1 in the normal function of these tissues, the availability of pharmacological tools for acutely manipulating the activity of Kir4.1 in genetically normal animals has been lacking. We therefore carried out a high-throughput screen of 76,575 compounds from the Vanderbilt Institute of Chemical Biology library for small-molecule modulators of Kir4.1. The most potent inhibitor identified was 2-(2-Bromo-4-iso-propylphenoxy)-*N*-(2,2,6,6-tetramethylpiperidin-4-yl)acetamide (VU0134992). In whole-cell patch clamp electrophysiology experiments, VU0134992 inhibits Kir4.1 with an IC_{50} of 0.97 μM and is 9-fold selective for homomeric Kir4.1 over Kir4.1/5.1 concatemeric channels (IC_{50}=9 μM) at -120 mV. In thallium (Tl^+) flux assays, VU0134992 is greater than 30-fold selective for Kir4.1 over Kir1.1, Kir2.1, and Kir2.2, is weakly active toward Kir2.3, Kir6.2/SUR1, and Kir7.1, and is equally active toward Kir3.1/3.2, Kir3.1/3.4, and Kir4.2. This potency and selectivity profile is superior to Kir4.1 inhibitors amitriptyline, nortriptyline, and fluoxetine. Medicinal chemistry identified components of VU0134992 that are critical for inhibiting Kir4.1. Patch clamp electrophysiology, molecular modeling, and site-directed mutagenesis identified pore-lining glutamate 158 and isoleucine 159 as critical residues for block of the channel. VU0134992 displayed a large free fraction in rat plasma (f_u = 0.213). Consistent with the known role of Kir4.1 in renal function, oral dosing of VU0134992 led to a dose-dependent diuresis, natriuresis, and kaliuresis in rats. Thus, VU0134992 represents the first *in vivo*-active tool compound for probing the therapeutic potential of Kir4.1 as a novel diuretic target for the treatment of hypertension.

Molecular Pharmacology Fast Forward. Published on June 12, 2018 as DOI: 10.1124/mol.118.112359
This article has not been copyedited and formatted. The final version may differ from this version.

INTRODUCTION

Kir4.1 inward rectifier potassium (Kir) channels (encoded by *KCNJ10*) are critical for regulating potassium (K^+) transport and electrolyte homeostasis in the central nervous system (CNS), retina, inner ear, and nephrons of the kidney (Hibino et al., 2010; Welling, 2016). In the brain and spinal cord, homotetrameric Kir4.1 channels are expressed almost exclusively in glia, oligodendrocytes, and astrocytes, although some evidence for neuronal expression has been reported (Zhang et al., 2011) (see below). Kir4.1 expression levels are variable between different brain and spinal cord regions, indicating the channel's contributions to CNS physiology are complex and anatomically heterogeneous(Nwaobi et al., 2016). Astroglial Kir4.1 channels are best known for their role in clearance, or "spatial buffering," of extracellular K^+ and glutamate in the CNS. By virtue of their prominent membrane expression and high open probability, Kir4.1 channels drive the membrane potential (Vm) of glial cells to negative voltages. When K^+ is released from active neurons, thereby locally depolarizing the Nernst equilibrium potential for K^+ with respect to the astrocyte V_m, an inwardly directed electrochemical driving force that promotes K^+ and glutamate uptake into astrocytes is generated (Djukic et al., 2007; Kofuji et al., 2002; Kucheryavykh et al., 2007; Olsen and Sontheimer, 2008).

Alterations in Kir4.1 expression and function are associated with a number of human diseases (Nwaobi et al., 2016). Autosomal recessive mutations in *KCNJ10* cause EAST (Epilepsy Ataxia Sensorineural deafness Tubulopathy) or SeSAME (Seizures Sensorineural deafness Ataxia Mental retardation Electrolyte imbalances) syndrome(Bockenhauer et al., 2009; Reichold et al., 2010; Scholl et al., 2009). The clinical presentation of EAST/SeSAME syndrome is readily explained by the loss of Kir4.1 function in the CNS, inner ear, and kidney. In two separate mouse models of Huntington's disease (i.e. R6/2 and Q175 mice), the functional expression of Kir4.1 in astrocytes is reduced, leading to elevated extracellular K^+ concentration and increase in neuronal excitability. Viral delivery of Kir4.1 channels to

Molecular Pharmacology Fast Forward. Published on June 12, 2018 as DOI: 10.1124/mol.118.112359
This article has not been copyedited and formatted. The final version may differ from this version.

striatal astrocytes prolongs the lifespan and attenuates some of the motor deficits in R6/2 mice (Tong et al., 2014). Epigenetic changes in Kir4.1 expression have been linked to Rett syndrome, a neurological disorder that affects cognitive, sensory, motor, and autonomic functions (e.g. cardiac function, digestion, and breathing). In most cases, Rett syndrome is caused by mutations in the methyl CpG binding protein 2 (MECP2) gene located on the X chromosome, which is responsible for the transcriptional regulation of dozens of genes, including *KCNJ10* (Nwaobi et al., 2016). Zhang and colleagues proposed that the overexpression of Kir4.1 homotetrameric channels in respiratory-related neurons from MecP2 mice leads to a reduction in CO_2/pH chemosensitivity and disruption of normal breathing (Zhang et al., 2011). This overexpression could be restricted to respiratory neurons since recent data from Olsen and colleagues suggest that there is a reduction in glial cell Kir4.1 from MeCP2 mice (Kahanovitch et al., 2018). An emerging body of literature has implicated Kir4.1 in autism spectrum disorder, SIDS, epilepsy, pain, and multiple sclerosis (Sicca et al., 2016; Sicca et al., 2011), although in most cases a clear mechanistic link between the channel and these diseases has not yet been established.

In polarized epithelial cells of the distal convoluted tubule (DCT) and cortical collecting duct (CCD), Kir4.1 is expressed on the basolateral (i.e. blood-facing) membrane, predominantly in a heteromeric complex with Kir5.1 (encoded by *KCNJ16*)(Lourdel et al., 2002; Welling, 2016; Zhang et al., 2014). Kir5.1 does not produce functional K^+ channels on its own, but serves to modify the functional (e.g. unitary conductance, activation kinetics, rectification) and regulatory (e.g. pH sensitivity) properties of Kir4.1-containing channels(Paulais et al., 2011; Pessia et al., 2001; Tucker et al., 2000). In the DCT, Kir4.1/5.1 channels 1) recycle K^+ ions across the basolateral membrane to sustain the activity of the basolateral Na^+/K^+/ATPase, which maintains a favorable chemical driving force for Na^+ reabsorption across the luminal (urine-facing) membrane by the Na^+/Cl^- co-transporter NCC, and 2) create a negative membrane potential that promotes Cl^- exit across the basolateral membrane. In the CCD, basolateral

Molecular Pharmacology Fast Forward. Published on June 12, 2018 as DOI: 10.1124/mol.118.112359
This article has not been copyedited and formatted. The final version may differ from this version.

Kir4.1/5.1 and Kir4.1 channels hyperpolarize the basolateral membrane potential and electrically coupled luminal membrane to promote Na^+ reabsorption via the Epithelial Na^+ Channel (ENaC). Thus, Kir4.1-containing channels play key roles in promoting NaCl reabsorption in the DCT and CCD of the nephron (Welling, 2016).

The lack of specific pharmacological tool compounds has slowed progress in exploring the function, integrative physiology, and in some cases therapeutic potential of Kir4.1, leading us to carry out a high-throughput screen (HTS) of 76,575 compounds for pharmacological modulators of Kir4.1. Here we report the discovery and characterization of VU0134992, the first *in vivo*-active inhibitor of renal Kir4.1 channels.

Molecular Pharmacology Fast Forward. Published on June 12, 2018 as DOI: 10.1124/mol.118.112359
This article has not been copyedited and formatted. The final version may differ from this version.

MATERIALS AND METHODS

Stable Cell Lines and Transient Transfection

Stably transfected monoclonal T-Rex-HEK-293 cell lines expressing Kir1.1, Kir2.2, Kir2.3, Kir4.1, Kir4.2, Kir6.2/SUR1, or Kir7.1-M125R from a tetracycline-inducible promoter were generated as described previously (Lewis et al., 2009; Raphemot et al., 2013; Raphemot et al., 2011; Swale et al., 2016). To promote cell surface expression and function of Kir4.2, lysine 110 was mutated to asparagine and the most distal 22 amino acids were deleted from the carboxyl-terminus (Kir4.2-K110N-Δ22), as described by Nichols and colleagues (Pearson et al., 2006). The day before Tl^+ flux assays, cells were plated at a density of 20,000 cells per well in black-walled, clear-bottomed, amine-coated 384-well plates (Purecoat™, Corning) in the presence of 1 µg/ml tetracycline to induce Kir channel expression. Constitutively expressing Kir3.1/3.2, Kir3.1/3.4 cells were used without any induction. Kir6.2/SUR1 was activated with 30 µM VU063 (Raphemot et al., 2014) for testing inhibitors. Transient transfections were performed using Lipofectamine-LTX according the manufacturer's instructions. The pcDNA3.1-Kir4.1-5.1 concatemer plasmid was obtained from Chung Jiang (Georgia State University) with permission from John Adelman (Oregon Health and Science University).

Kir4.1 Primary Screen

Tl^+ flux assays were performed as described previously (Lewis et al., 2009; Raphemot et al., 2013; Raphemot et al., 2011; Swale et al., 2016) with modifications to reagents optimized per cell line as noted below. Briefly, cells cultured overnight 37 °C and 5% CO_2 in 384-well plates were loaded with the thallium-sensitive dye Thallos-AM (TEFLabs, Austin, TX) in ambient conditions, washing before and after dye using Hank's Balanced Salt Solution/20mM HEPES (assay buffer). Media and buffer exchange was performed on the ELx405 plate washer (BioTek). Dye loaded cells were then transferred to the Hamamatsu Functional Drug Screening System 6000 (FDSS6000; Hamamatsu, Tokyo, Japan) or

Molecular Pharmacology Fast Forward. Published on June 12, 2018 as DOI: 10.1124/mol.118.112359
This article has not been copyedited and formatted. The final version may differ from this version.

Panoptic kinetic imaging plate reader (Wavefront Bioscience, Franklin, TN, USA). Both instruments collect live measurements at 1 Hz (480/40 nm excitation and 540/40 nm emission) during simultaneous 384-well pipetting of 10 µM small-molecules (0.1% DMSO assay buffer) or control (100 µM fluoxetine). Cells are treated 20 minutes, continuing ambient conditions, before adding 5X Tl^+ stimulus buffer (125 mM $NaHCO_3$, 1 mM $MgSO_4$, 1.8 mM CaSO4, 5 mM glucose, 20 mM HEPES, and 1.8 – 6 mM Tl_2SO_4) to each well to initiate Tl^+ flux. Screening data were collected into a custom database and data reduction software application to merge individual compounds with the associated values on a well-to-well, then plate-by-plate basis. Fluorescence values for individual wells were normalized by dividing each data point for that well by the initial data point (F/F_0). After normalization of all wells, the fluorescence data (i.e. fluorescence vs. time) from each of the designated vehicle-control wells was averaged and this averaged control wave was subtracted from all wells on the plate to yield normalized, vehicle control-subtracted data. Fluorescence amplitudes (max-min) were extracted from the control-subtracted wells over a range from 0-200 seconds. Alternatively, the slope 5-20 sec after Tl^+ addition was calculated. Hit selections were made by analysis on a per plate basis evaluating 3 standard deviations from the mean of the compound population. Compounds that were tested in dose-response were calculated as above, and reduced values were then plotted with GraphPad Prism version 5.01 (GraphPad Software, San Diego, CA) to generate estimated potencies of concentration response curves (CRC) fit using a four-parameter logistic model of non-linear regression analysis.

Site-Directed Mutagenesis

Mutations in Kir4.1 were introduced using a QuickChange II Site-Directed Mutagenesis kit (Agilent Technologies) according to the manufacturer's instructions. The complete cDNA was sequenced to verify introduction of the intended codon changes.

Molecular Pharmacology Fast Forward. Published on June 12, 2018 as DOI: 10.1124/mol.118.112359
This article has not been copyedited and formatted. The final version may differ from this version.

Patch Clamp Electrophysiology

HEK-293T cells were transfected with wild type or mutant pcDNA5-Kir4.1 (1µg) and pcDNA3.1-EGFP (0.5µg; transfection marker) using Lipofectamine LTX reagent according to the manufacturer's instructions. The cells were dissociated the following day and plated on poly-L-lysine-coated coverslips and allowed to recover for at least 1h in a 37 °C 5% CO_2/95% air incubator before starting experiments. Patch clamp experiments were performed essentially as described previously (Raphemot et al., 2013). Briefly, patch electrodes (2-3MΩ) were filled with an intracellular solution containing 135 mM KCl, 2 mM $MgCl_2$, 1 mM EGTA, 10 mM HEPES-free acid, and 2 mM Na_2ATP (Roche Diagnostics), pH 7.3, 275 mOsmol/kg water. The standard bath solution contained 135 mM NaCl, 5 mM KCl, 2 mM $CaCl_2$, 1 mM $MgCl_2$, 5 mM glucose, and 10 mM HEPES free acid, pH 7.4. Macroscopic currents were recorded under whole-cell voltage-clamp conditions using an Axopatch 200B amplifier (Molecular Devices, Sunnyvale, CA). Cells were voltage clamped at a holding potential of −75 mV and stepped every 5 s to −120 mV for 200 msec before ramping to 120 mV at a rate of 1.2 mV/msec. Data were collected at 5 kHz and filtered at 1 kHz. Data acquisition and analysis were performed using the pClamp 9.2 software suite (Molecular Devices, Sunnyvale, CA). Pharmacology experiments were terminated by applying 2 mM barium (Ba^{2+}) chloride to measure leak current. Cells exhibiting <90% block by Ba^{2+} were excluded from analysis. The mean current amplitude recorded over five successive steps to −120 mV in WT control or mutants at single concentration were expressed as mean ± SD. Statistical analysis was performed using one-way ANOVA with Bonferroni's multiple comparisons test with statistical significance defined at $P < 0.05$. IC_{50} values were determined by fitting the Hill equation to concentration-response curves (CRCs) using variable-slope nonlinear regression analyses. All the analysis was performed with GraphPad Prism version 5.01 (GraphPad Software, San Diego, CA).

Molecular Pharmacology Fast Forward. Published on June 12, 2018 as DOI: 10.1124/mol.118.112359
This article has not been copyedited and formatted. The final version may differ from this version.

Homology Modeling of Kir4.1

The Kir4.1 sequence (residues 28-360) was threaded onto the Kir2.2 crystal structure (PDB 3JYC) based on a sequence alignment generated by ClustalW. The sequence identity between Kir4.1 and Kir2.2 is 43.3%. Transmembrane segments for Kir4.1 were predicted using the OCTOPUS topology prediction web server (http://octopus.cbr.su.se/). Missing coordinates in the threaded Kir4.1 model were reconstructed using Rosetta with fragment insertion from the fragment libraries generated by the Rosetta server (Leaver-Fay et al., 2007). The modeling pipeline utilized RosettaMembrane (Barth et al., 2007) and RosettaSymmetry (King et al., 2012) in the Rosetta revision 58019. Loops were closed using the cyclic coordinate descent (CCD) algorithm and refined using Kinematic loop closure (KLC) from the Rosetta Loop Modeling application (Mandell et al., 2009). 1000 models were generated and the top eight models by score and RMSD to Kir2.2 (models 1-8) were further relaxed using FastRelax in the Rosetta relax application producing 100 models each. The top 3 models from parent models 1, 2, 3, 5 and 7 were chosen for ligand docking studies.

Docking VU0134992 in the Kir4.1 Channel Pore

VU0134992 was manually placed in a coordinate frame that corresponds to the pore cavity below the selectivity filter of Kir4.1. VU0134992 conformers were generated usingBCL::Conf (Kothiwale et al., 2015). The top 15 homology models described above were used for ligand binding studies with RosettaLigand (Meiler and Baker, 2006), producing 7500 VU0134992-Kir4.1 complexes. The top 10% of 750 models by Rosetta interface score were analyzed for favorable residue interactions (better than -1 REU) and highest frequency interaction between residues of Kir4.1 and VU0134992.

Molecular Pharmacology Fast Forward. Published on June 12, 2018 as DOI: 10.1124/mol.118.112359
This article has not been copyedited and formatted. The final version may differ from this version.

Chemical Synthesis

Synthesis and Characterization of VU0134992

Synthetic scheme of VU0134992 is shown in Supplemental Figure S1 as an example of general synthetic scheme. Experimental procedure for VU0134992 is described below. Specific synthetic schemes for selected compounds are also shown in supplemental information (Figures S2 and S3).

2-Bromo-4-iso-propylphenol (2): To a solution of 4-*iso*-propylphenol (2.00 g, 14.7 mmol) in CH_3CN (30 mL) was added *N*-bromosuccinimide (2.88 g, 16.2 mmol) at 0^oC. After a resulting greenish solution was stirred at 0^oC for 1.5 hours, ice/$NaHCO_3$-*aq* was added to the reaction mixture which was extracted with ethyl acetate twice. Combined organic extracts were washed with brine and dried over $MgSO_4$. The filtrate was evaporated under reduced pressure to give crude residue which was purified on silica gel chromatography (hexane/ethyl acetate) to yield 2-bromo-4-*iso*-propylphenol **2** (723 mg (content 618 mg), 20% yield) as a pale yellow oil. Crude fraction collected was purified by Gilson HPLC separation system using (0.1% TFA in water)/CH3CN as an eluent. Extraction from the collected fraction with DCM gave another batch of **2** (1.06 g (content 1.02 g), 32% yield) as a pale reddish oil. Total yield was 52%.

2-Chloro-N-(2,2,6,6-tetramethylpiperidin-4-yl)acetamide hydrochloride (4): To a solution of 4-amino-2,2,6,6-tetramethylpiperidine **3** (2.345 g, 15.0 mmol) in DCM (30 mL) was added chloroacetyl chloride (1.19 mL, 15.0 mmol) at 0^oC. After a resulting white suspension was stirred at 0^oC for 40 min, precipitates were collected by filtration to yield 2-chloro-*N*-(2,2,6,6-tetramethylpiperidin-4-yl)acetamide hydrochloride **4** (4.052 g (content 3.908 g), 97% yield).

Molecular Pharmacology Fast Forward. Published on June 12, 2018 as DOI: 10.1124/mol.118.112359
This article has not been copyedited and formatted. The final version may differ from this version.

2-(2-Bromo-4-iso-propylphenoxy)-N-(2,2,6,6-tetramethylpiperidin-4-yl)acetamide (VU0134992): To a solution of **2** (935 mg, 4.35 mmol) in DMF (30 mL) was added **4** (975 mg, 3.62 mmol), Cs_2CO_3 (2.95 g, 9.05 mmol) and NaI (179 mg, 1.19 mmol) at ambient temperature. After a resulting white suspension was stirred at 50^{o}C for 18h hour, the reaction mixture was poured into cold 1 mol/L NaOH-*aq* (120 mL) and it was extracted with DCM three times (1st: 50 mL, 2nd: 50 mL, 3rd: 30 mL). Combined organic extracts were washed with brine (40 mL) and dried over $MgSO_4$. The filtrate was evaporated under reduced pressure. The residue was purified by Gilson HPLC separation system using (0.1% TFA in water)/CH3CN as an eluent. Desired fractions were collected and concentrated up to about half amount. CH_3CN was added to the aqueous solution until precipitates were formed (ratio of water:CH_3CN was about 1:2). After the precipitate was collected by filtration, it was extracted with DCM from 1 mol/L NaOH-*aq* three times. Combined organic extracts were dried over $MgSO_4$. The filtrate was evaporated under reduced pressure to yield 2-(2-bromo-4-*iso*-propylphenoxy)-*N*-(2,2,6,6-tetramethylpiperidin-4-yl)acetamide **VU0134992** (1.16 g, 78% yield) as a white powder. ^{1}H NMR (400.1 MHz, $CDCl_3$): 7.42 (d, J = 1.7 Hz, 1H), 7.13 (dd, J = 8.4, 1.7 Hz, 1H), 6.80 (d, J = 8.4 Hz, 1H), 6.74 (d, J = 8.0 Hz, 1H), 4.48 (s, 2H), 4.39-4.30 (m, 1H), 2.85 (sept, J = 6.9 Hz, 1H), 1.96-1.92 (m, 2H), 1.27 (s, 6H), 1.22 (d, J = 6.9 Hz, 6H), 1.14 (s, 6H), 1.03-0.97 (m, 2H). ^{13}C NMR (100.6 MHz, $CDCl_3$): 166.87, 151.81, 144.44, 131.41, 126.90, 113.87, 112.10, 68.51, 51.17, 45.27, 42.47, 35.10, 33.38, 28.73, 24.12. LCMS: R_T = 0.912 min, *m/z* = 411 $[M + H]^+$. HRMS calculated for $C_{20}H_{31}BrN_2O_2$ $[M^+]$, 410.1569; found 410.1571.

Drug Metabolism and Pharmacokinetics (DMPK)

Detailed methods for *in-vitro* and *in vivo* DMPK analyses are described in Supplemental Methods.

Molecular Pharmacology Fast Forward. Published on June 12, 2018 as DOI: 10.1124/mol.118.112359
This article has not been copyedited and formatted. The final version may differ from this version.

Metabolic Cage Studies

All studies involving animals were approved by Institutional Animal Care and Use Committee. Metabolic cage studies were done as described previously (Kharade et al., 2015). Briefly, male Sprague-Dawley rats (250-300 g) were allowed to acclimatize to single housing in metabolic cages for 2h before an experiment. Access to food and water was restricted during the entire experiment. Rats were given drug VU0134992 or vehicle (10% ethanol + 40% PEG400 + 50% saline) by oral gavage (PO). After 30 mins, voiding was induced by giving each animal a saline load (18 ml/kg by oral gavage), and urine was collected at 2h, 4h and 6h time points. Urine volumes were measured, centrifuged, aliquoted, and frozen at -80°C until analyzed. Urine Na^+ and K^+ concentrations were measured by flame photometry (Instrumentation Laboratories model 943, Lexington, MA). The total number of moles of Na^+ or K^+ excreted over the 4 hours was normalized to animal body weight (i.e. µmol/100 g/4h). The data are expressed as the mean ± SD and was analyzed using one-way ANOVA with Bonferroni's multiple comparisons test with statistical significance defined at $P < 0.05$.

Molecular Pharmacology Fast Forward. Published on June 12, 2018 as DOI: 10.1124/mol.118.112359
This article has not been copyedited and formatted. The final version may differ from this version.

RESULTS

Discovery of VU0134992

76,575 structurally diverse small-molecules from the Vanderbilt Institute of Chemical Biology library were screened against Kir4.1 using a Tl^+ flux assay that we have described previously (Raphemot et al., 2013). Briefly, the assay reports the inwardly directed movement of Tl^+ through the ion conduction pore of Kir4.1 using the intracellular, Tl^+-sensitive dye Thallos. The mean Z' plate statistic for the primary screen was 0.78, indicating the assay's performance was robust and reproducible, and a hit rate of 0.8%. We selected 640 hit compounds resupplied from the vendor for confirmation and counter screening against induced and uninduced cells. 58 hits inhibited Tl^+ flux in tetracycline-induced T-Rex-HEK-293-Kir4.1 cells in duplicate testing at 10 μM. Screening against uninduced cells identified 42 compounds that inhibited endogenous Tl^+ flux pathways expressed in T-Rex-HEK293 cells. This left 16 authentic inhibitors of Kir4.1 (0.02% success rate). We focused on VU0134992 because of its superior potency, selectivity, and chemical tractability. In gold-standard patch clamp electrophysiology experiments, VU0134992 markedly inhibited Kir4.1 at 3 μM with an IC_{50} of 0.97 μM (95% CI, 0.5 μM to 1.7 μM) (Fig. 1). Because Kir4.1 forms heteromeric channels with Kir5.1 in the kidney (Lachheb et al., 2008; Tucker et al., 2000; Zhang et al., 2015; Zhang et al., 2014), we evaluated the sensitivity of Kir4.1-5.1 concatemeric channels to VU0134992. As shown in Fig. 1, VU0134992 inhibits Kir4.1-5.1 concatemeric channels with an IC_{50} of 9.05 μM (95% CI 7.4 μM to 11.1 μM) at -120 mV, providing approximately 9-fold selectivity toward Kir4.1 over Kir4.1-5.1 channels at this test potential. The IC_{50} values for inhibition of outward currents through Kir4.1 and Kir4.1-5.1 at +120 mV were 1.2 μM (95% CI – 0.97 μM to 1.6 μM) and 26.8 μM (95% CI 18.2 μM to 39.8 μM)(22-fold selectivity).

Molecular Pharmacology Fast Forward. Published on June 12, 2018 as DOI: 10.1124/mol.118.112359
This article has not been copyedited and formatted. The final version may differ from this version.

VU0134992 Selectivity

The selectivity of VU0134992 for Kir4.1 versus 9 other members of the Kir channel family was evaluated at concentrations ranging from 0.3 nM to 30 μM in 11-point CRC experiments, using established Tl^+ flux assays (Swale et al., 2016). The results are summarized in Table 1. VU0134992 exhibited no apparent activity toward Kir1.1, Kir2.1, or Kir2.2, and caused only partial inhibition of Kir2.3 (73% inhibition at 30 μM), Kir6.2/SUR1 (12% inhibition at 30 μM), and Kir7.1 (15% inhibition at 30 μM,). However, upon further evaluation, we found that VU0134992 inhibits Kir3.1/3.2 (92% inhibition at 30 μM, IC_{50}=2.5 μM), Kir3.1/3.4 (92% inhibition at 30 μM, IC_{50}=3.1 μM), and Kir4.2 (100% inhibition at 30 μM, IC_{50}=8.1 μM with approximately the same efficacy and potency that VU0134992 inhibits Kir4.1 (100% at 30 μM, IC_{50}=5.2 μM). The rightward shift in Kir4.1 IC_{50} derived from Tl^+ flux experiments compared to electrophysiology experiments is commonly observed with other Kir channels (Bhave et al., 2011; Raphemot et al., 2013; Raphemot et al., 2011; Swale et al., 2016).

The antidepressants amitriptyline, nortriptyline, and fluoxetine have been used to inhibit Kir4.1 activity in heterologous expression and native cell systems (Furutani et al., 2009; Ohno et al., 2007; Su et al., 2007). However, these drugs have never been systematically evaluated for selectivity toward Kir4.1 over several closely related Kir channels in a single, systematic study. Toward this end, and to provide a comparison for VU0134992, we evaluated the potency and efficacy of amitriptyline, nortriptyline, and fluoxetine toward Kir1.1, Kir2.1, Kir2.3, Kir3.1/3.2, Kir3.1/3.4, Kir4.1, Kir4.2, Kir6.1/SUR1, and Kir7.1-M125R, in 11-point CRCs at concentrations up to 90 μM. As summarized in Table 1, all 3 drugs exhibited weak and non-specific activity toward most members of the Kir channel family at concentrations that also inhibit Kir4.1. Thus, VU0134992 is more potent and selective than amitriptyline, nortriptyline, and fluoxetine toward Kir4.1 channels.

Molecular Pharmacology Fast Forward. Published on June 12, 2018 as DOI: 10.1124/mol.118.112359
This article has not been copyedited and formatted. The final version may differ from this version.

VU0134992 Interacts with E158 and I159 to Block the Kir4.1 Channel Pore

A common mechanism by which small-molecules inhibit Kir channels is through blockade of the ion-conduction pore (Furutani et al., 2009; Kharade et al., 2017; Swale et al., 2014; Swale et al., 2016). Some pore-blocker exhibit voltage-dependent "knock-off" behavior at test potentials more negative than the Nernst K^+ equilibrium potential difference. We therefore evaluated the voltage- and K^+-dependence of VU0134992 inhibition of Kir4.1 to begin identifying the VU0134992 binding site. As shown in Fig. 2A, 30 μM VU0134992 fully inhibited Kir4.1-mediated outward and inward currents across all test potentials when cells were bathed in a solution containing 5 mM K^+ and patch clamped using an internal solution containing 135 mM K^+ (Nernst equilibrium potential = -83 mV). However, when extracellular K^+ concentration was raised to 50 mM K^+ (Nernst equilibrium potential = -25 mV), we observed a time-dependent knock-off of VU0134992 at strong hyperpolarizing potentials (Fig. 2) and statistically significant reduction of block between -120 mV and -100 mV (Fig. 2). These data suggested that the VU0134992 binding site is indeed located within the Kir4.1 channel pore.

To identify pore-lining residues that participate in VU0134992 binding in the pore, we generated a comparative homology model of Kir4.1 based on the human Kir2.2 crystal structure and employed *in silico* docking to identify energetically favorable VU0134992 docking sites within the channel pore. Analysis of the top scoring VU0134992-Kir4.1 complexes by Rosetta interface score identified 4 pore-lining residues in Kir4.1 that 1) showed high frequency (>10% out of 750 models) interactions with VU0134992 and 2) were different between Kir4.1 and Kir1.1. These residues are in the rank order of glutamate (E)158 (39.5% of interactions) > threonine (T)162 (37.3% of interactions) > T155 (10.1 % of interactions) > isoleucine (I)159 (10.0 % of interactions). The interactions are a combination of hydrogen bonds and van der Waals interactions (Fig. 3A)The homology model in Fig. 3A shows the predicted location of the VU0134992 in the membrane-spanning pore (right), whereas the close-up view

Molecular Pharmacology Fast Forward. Published on June 12, 2018 as DOI: 10.1124/mol.118.112359
This article has not been copyedited and formatted. The final version may differ from this version.

(left) identifies close interactions of VU0134992 with E158, the top-scoring residue. Interactions with E158 are dominated by hydrogen bonds. However, several van der Waals contacts exist in addition.

We mutated these four amino acids to the corresponding residues in Kir1.1, which is virtually insensitive to VU0134992 (Fig. 3B-E), and measured the inhibition of the mutant channels to 3 μM VU0134992 by whole-cell patch clamp electrophysiology. As shown in Figure 3B, 3 μM VU0134992 inhibited inward current at -120 mV carried by WT Kir4.1 by 85.9 ± 11 % (n = 12). In striking contrast, mutation of E158 to asparagine (E158N) dramatically reduced the sensitivity of the channel to VU0134992 (0.4 ± 12 % inhibition, n = 8; IC_{50} ~235 μM with only 38.2 ± 14.7 % inhibition at 30 μM) at -120mV. To determine if this loss of sensitivity is caused by alteration of side chain charge or structure, we evaluated channels in which E158 was mutated to either glutamine (E158Q) or aspartate (E158D). Both mutant channels exhibited a complete loss of sensitivity to 3 μM VU0134992 and a large rightward shift in IC_{50} (Kir4.1-E158Q ~28 mM; Kir4.1-E158D = no fit), suggesting that changes in side-chain structure at position 158 are sufficient to affect VU0134992 block. Mutation of I159 to serine (I159S) caused a complete loss of block by 3 μM VU0134992 and large rightward shift in the CRC (9.5 ± 7.7 %, n=6; IC_{50} ~199 μM and 77±20 % inhibition at 30 μM; Fig. 3B, D). Kir4.1-T155V channels were not functional (NF) and therefore could not be evaluated. We also mutated nearby residues T162 to cysteine (T162C), T164 to alanine (T164A) and F165 to isoleucine (F165I), however neither mutation affected VU0134992 sensitivity.

VU0134992 Structure-Activity Relationships

We employed medicinal chemistry in an effort to improve the potency of VU0134992 and establish its structure-activity relationships (SAR) for inhibition of Kir4.1. No modifications made to the scaffold of VU0134992 improved its activity toward Kir4.1. It was revealed that VU0134992 bears fundamental

Molecular Pharmacology Fast Forward. Published on June 12, 2018 as DOI: 10.1124/mol.118.112359
This article has not been copyedited and formatted. The final version may differ from this version.

components for inhibition of Kir4.1 channels (Supplemental Tables. S1-3). An overview of the SAR is shown in Fig. 4. While flat SAR was observed at the 4-position in the left-hand part for inhibitory activity of Kir4.1 with IC_{50} of 3.0 – 9.6 μM in the thallium flux assay (methyl, ethyl, *iso*-propyl (**VU0134992**), *tert*-butyl, chloro and phenyl substituents), the mono-bromine atom at the 2-position was critical for the potency (Not only F, Cl, H substituents for Br were all inactive (No Fit) but also addition of Br and Cl at the 6-position resulted in notable decrease in potency) (Table. S1). While the linker modification was tolerated, such as incorporation of dimethyl substituents at α-position of the amide (Table. S3), all of modifications in the right-hand part made the compound noticeably less active (Table. S2).

VU0134992 Serum Binding, Clearance, and Blood-Brain-Barrier Permeability

VU0134992 displayed a large free fraction in rat plasma (f_u = 0.213), modest fraction unbound in rat brain (f_u = 0.013), moderate predicted hepatic clearance in human (13.4 mL/min/kg), and high predicted hepatic clearance in rat (60.5 mL/min/kg) liver microsomes. A good *in vitro:in vivo* correlation was noted, with clearance above cardiac output (CLp > 1000 mL/min/kg), and with a short half-life ($t_{1/2}$ = 10.6 min) driven by a large volume of distribution at steady state (V_{ss} = 13.5 L/kg). In a standard rat plasma:brain level (PBL) cassette, which is routinely used to rapidly screen the brain distribution potential of compounds, VU0134992 levels were below the limit of quantification (BLQ) in brain. We also measured plasma and brain levels following an oral dose of 50 mg/kg, a dosing regimen that was used in subsequent metabolic cage studies (see below). Total VU0134992 brain and plasma concentrations were 0.94 μM and 0.76 μM (Kp = 1.2), respectively, whereas unbound VU0134992 concentrations in brain and plasma were 0.012 μM and 0.16 μM (Kp,uu = 0.08).

Molecular Pharmacology Fast Forward. Published on June 12, 2018 as DOI: 10.1124/mol.118.112359
This article has not been copyedited and formatted. The final version may differ from this version.

Effects of VU0134992 on Renal Fluid and Electrolyte Excretion

Given the important role of Kir4.1 in renal Na^+ reabsorption and K^+ secretion, we have postulated that small-molecule inhibitors of Kir4.1 will induce diuresis, natriuresis, and kaliuresis (Denton et al., 2013). To test this hypothesis, we evaluated the effects of VU0134992 on renal function in volume-loaded Sprague-Dawley rats. The rats were administered with either vehicle or different doses of VU0134992 followed by volume-loading. The effects of VU0134992 on urine output are summarized in Fig. 5. Consistent with the hypothesis, oral administration of VU0134992 led to a statistically significant increase in urine output as compared to vehicle at doses of 50 mg/kg and 100 mg/kg. Urine Na^+ and K^+ concentrations were measured to determine how VU0134992 alters electrolyte transport along the nephron. As shown in Figs. 5B and 5C, VU0134992 statistically significantly ($P<0.05$) increased urinary Na^+ as well as K^+ excretion at doses of 50 mg/kg and 100 mg/kg compared to vehicle-treated control animals.

Molecular Pharmacology Fast Forward. Published on June 12, 2018 as DOI: 10.1124/mol.118.112359
This article has not been copyedited and formatted. The final version may differ from this version.

DISCUSSION

Here we report the discovery and characterization of VU0134992, the first Kir4.1 K^+ channel inhibitor to emerge from a high-throughput screening campaign. VU0134992 affords approximately 9-22 fold selectivity between homotetrameric Kir4.1 and heterotetrameric Kir4.1/5.1 channels when evaluated at -120 mV and +120 mV, respectively, a property that could be useful for sorting out the relative contribution of these two channel populations in native cells. To our knowledge, VU0134992 is the first subtype-preferring Kir4.1 inhibitor to be reported. Efforts to understand the molecular basis of this selectivity and to identify VU0134992 analogs with improved potency and selectivity toward Kir4.1 and Kir4.1/5.1 channels are underway.

The pharmacology of Kir4.1 has been primarily limited to inorganic cations (e.g. Ba^{2+}, cesium) and anti-depressants that have relatively weak off-target activity toward Kir4.1. A summary of published small-molecule Kir4.1 inhibitors, their intended drug targets, and IC_{50} values for Kir4.1 are shown in Table 2. The tricyclic antidepressant (TCA) drugs nortriptyline, amitriptyline, desipramine, and imipramine were the first small-molecules shown to inhibit Kir4.1 (Su et al., 2007). The IC_{50} for inhibition by nortriptyline is 16 μM and 38 μM at test potentials of +30 mV and -110 mV, respectively, and block is relieved upon elevation of extracellular K^+ concentration. Kir4.1 is also inhibited by the Selective Serotonin Reuptake Inhibitor (SSRI) drugs fluoxetine, sertraline, and fluvoxamine (Ohno et al., 2007). Similar to nortriptyline, block by fluvoxamine is voltage-dependent and reduced by membrane hyperpolarization. Mutational analysis revealed that Kir4.1 inhibition by fluoxetine and nortriptyline requires T128 and E158 (Furutani et al., 2009). More recently, the anti-malarial drugs quinacrine and chloroquine were also shown to inhibit Kir4.1 in a voltage-dependent manner involving interactions with T128 and E158 (Marmolejo-Murillo et al., 2017a; Marmolejo-Murillo et al., 2017b). The most potent intracellular pore blocker of Kir4.1 is currently pentamidine (Arechiga-Figueroa et al., 2017).

Molecular Pharmacology Fast Forward. Published on June 12, 2018 as DOI: 10.1124/mol.118.112359
This article has not been copyedited and formatted. The final version may differ from this version.

When applied to the intracellular face of excised membrane patches, pentamidine inhibits Kir4.1 at +80 mV with an IC_{50} of 97 nM. Similar to the other inhibitors, Kir4.1 block by pentamidine requires interactions with T127, T128, and E158. Unfortunately, pentamidine is a poor inhibitor of Kir4.1 in the whole-cell configuration (i.e. ~25% inhibition by 1 μM pentamidine after 20 mins) and presumably intact cells. Thus, pentamidine is a useful tool for probing the structure of the intracellular pore, but will be limited as an *in vitro* and *in vivo* tool compound for exploring the physiology and druggability of Kir4.1. In the present study, we found that inhibition of Kir4.1 by VU0134992 exhibited voltage-dependent knockoff behavior at hyperpolarized test potentials that is consistent with block of the inner pore cavity. We employed *in silico* docking calculations to guide mutagenic analysis of potential pore-lining binding sites in Kir4.1. Mutation of two of the top-scoring residues led to a severe (E158N/Q/D, I159S) loss of VU0134992 sensitivity, lending experimental validation for this computational approach to identifying small-molecule binding sites in the Kir4.1 channel pore. Interestingly, VU0134992 inhibited Kir3.1/3.2 and Kir3.1/3.4 channels with similar potencies. Because Kir3.2 and Kir3.4 have asparagine (N) residues at positions equivalent to E158 in Kir4.1, we postulate that this cross-activity is due to D173 in Kir3.1 (also equivalent to Kir4.1-E158) in heteromeric Kir3.1/3.2 and Kir3.1/3.4 channels.

Kir4.1 was the first K^+ channel to be immunolocalized to the basolateral membrane of renal epithelial cells (Ito et al., 1996). The “silent” subunit, Kir5.1, was subsequently co-localized with Kir4.1 in the nephron, which, taken together with heterologous expression experiments showing that Kir4.1 and Kir5.1 form heteromeric channel complexes, suggested that the native channel subtype in the nephron is a Kir4.1-5.1 heteromer. Patch clamp experiments on isolated nephron segments have identified a predominant ~40-picoSiemens (pS) basolateral K^+ current that exhibits biophysical and regulatory properties that resemble heterologously expressed Kir4.1-5.1 (Lachheb et al., 2008) and is absent in

Molecular Pharmacology Fast Forward. Published on June 12, 2018 as DOI: 10.1124/mol.118.112359
This article has not been copyedited and formatted. The final version may differ from this version.

KCNJ10-knockout mice (Zhang et al., 2015; Zhang et al., 2014), and a less common ~20 pS current that resembles homomeric Kir4.1 (Zaika et al., 2013a; Zhang et al., 2013). Both of these channels appear to play important physiological roles in the nephron (see below).

The basolateral K^+ conductance of the cortical TAL is carried by a 40-pS channel that is likely comprised of Kir4.1-5.1 heteromeric channels, and an 80-pS channel possibly carried by Na^+-activated K^+ (K_{Na}) channels (Fan et al., 2015; Zhang et al., 2015)(Fig. 6). Genetic ablation of *KCNJ10* has no effect on the basolateral membrane potential in the TAL due to compensatory upregulation of the 80-pS channel (Zhang et al., 2015), suggesting that depolarization of the basolateral membrane potential in the TAL is unlikely to contribute to salt wasting in *KCNJ10*-knockout mice and EAST/SeSAME syndrome patients (Bockenhauer et al., 2009; Scholl et al., 2009). Interestingly, however, inhibition of the 40-pS channel with Ba^{2+} reduces the activity of basolateral ClC-Kb Cl^- channels through mechanisms that are currently unclear but do not appear to involve membrane depolarization (Fan et al., 2015). These data suggest that the natriuretic and diuretic effects of VU0134992 could result at least in part through inhibition of NaCl reabsorption in the TAL, as follows. NaCl reabsorption from the tubule fluid in the TAL is mediated by the electroneutral, loop diuretic-inhibitable, Na^+-K^+-$2Cl^-$ co-transporter, NKCC2 (Fig. 6). Na^+ is then pumped across the basolateral membrane through the Na^+-K^+-ATPase, and Cl^- is conducted out of the cell through ClC-Kb Cl^- channels. The indirect inhibition of ClC-Kb channels with VU0134992 should increase intracellular Cl^- concentrations and thereby reduce the inwardly directed driving force for Cl^- and coupled Na^+ and K^+ transport by NKCC2. In addition, basolateral K^+ secretion provides substrate K^+ ions that are needed to maintain the activity of the Na^+-K^+-ATPase. Provided that the 80-pS channel cannot compensate for the pharmacological inhibition of 40-pS Kir4.1-5.1 channels, VU0134992 should also slow the activity of the Na^+-K^+-ATPase, increase intracellular Na^+, and further reduce the chemical driving force for NaCl reabsorption via NKCC2 (Fig. 6).

Molecular Pharmacology Fast Forward. Published on June 12, 2018 as DOI: 10.1124/mol.118.112359
This article has not been copyedited and formatted. The final version may differ from this version.

NaCl reabsorption in the DCT is mediated by the luminal membrane, electroneutral, thiazide-sensitive Na^+-Cl^- co-transporter, NCC (Fig. 6). A rapidly developing body of evidence indicates that heterotetrameric Kir4.1-5.1 channels, which dominate the basolateral K^+ conductance in the DCT, are critical regulators of NCC expression and activity (Penton et al., 2016; Zhang et al., 2014). Deletion of *KCNJ10* in mice depolarizes the basolateral membrane potential, inhibits the basolateral Cl^- conductance, and reduces the expression of NCC (Zhang et al., 2014). Furthermore, Penton and colleagues demonstrated that application of Ba^{2+} to kidney slices induced dephosphorylation and hence inhibition of NCC. Taken together, these data are consistent with a model in which inhibition of Kir4.1 activity increases intracellular Cl^- concentration, which, in turn, inhibits NCC function through the Cl^--sensitive WNK/SPAK kinase pathway (reviewed in (Su and Wang, 2016). Ongoing studies are testing if VU0134992 administration induces the dephosphorylation of NCC in mice.

In the mouse CCD, Kir4.1 is expressed as a common 40-pS Kir4.1/5.1 current and a scarce 20-pS current carried by homomeric Kir4.1 channels (Zaika et al., 2013b)(Fig. 6). Although the 40 pS channel is more common, the 20 pS current has a higher open probability and thus likely plays an important role in setting the resting membrane potential. In principle cells of the CCD, activation of insulin receptors stimulates the activity of Kir4.1-containing channels, which, in turn, increases the electrochemical driving force for Na^+ reabsorption by the epithelial sodium channel (ENaC). In contrast, inhibition of Kir4.1 and Kir4.1/5.1 channels by dopamine acting on D2-like receptors leads to reduced Na^+ reabsorption via ENaC (Zaika et al., 2013a). These data suggest that VU0134992 induces natriuresis at least in part through inhibition of Kir4.1-containing channels expressed in the CCD (Fig. 6).

Molecular Pharmacology Fast Forward. Published on June 12, 2018 as DOI: 10.1124/mol.118.112359
This article has not been copyedited and formatted. The final version may differ from this version.

The diuretic and natriuretic responses induced by VU0134992 were accompanied by increases in urinary K^+ excretion. In this regard, the renal actions of VU0134992 are reminiscent of those caused by loop or thiazide diuretics. The simplest interpretation is that the increased volume and Na^+ load delivered to the distal nephron, secondary to inhibition of Na^+ reabsorption in the TAL and/or DCT, stimulates K^+ secretion via flow-stimulated large-conductance "BK" K^+ channels expressed in the CCD (Liu et al., 2007; Liu et al., 2009). These responses are different from those induced by inhibitors of the Renal Outer Medullary K^+ channel, ROMK (Kir1.1), another emerging diuretic target in the Kir channel family (Denton et al., 2013). We and others have shown that ROMK inhibition evokes diuresis and natriuresis without causing K^+ wasting (Garcia et al., 2014; Kharade et al., 2015; Zhou et al., 2017). The K^+-sparing effect appears to result predominantly from inhibition of K^+ secretion in the TAL with a relatively minor effect on distal K^+ secretion (Kharade et al., 2015).

In conclusion, we have identified and characterized a moderately potent and selective inhibitor of Kir4.1 that exhibits preference for the homotetrameric channel over heteromeric Kir4.1-5.1 channels. Oral administration of VU0134992 induces dose-dependent increases in urine volume, Na^+ excretion, and K^+ excretion in rats. We propose that the observed changes in renal excretion of water and electrolytes results from inhibition of basolateral Kir4.1-containing channels somewhere along the nephron. The low unbound VU0134992 brain-to-plasma ratio ($K_{p,uu}$ = 0.08) also supports the idea that the effects of VU0134992 on renal excretion is due to inhibition of Kir4.1 channels in the kidney and not in the brain. Future studies will be aimed at characterizing the activity of VU0134992 on electrolyte transport in the TAL, DCT, and CCD. The data presented herein raise the intriguing possibility that inhibition of basolateral Kir4.1-containing channels could be an effective way to lower blood pressure in hypertensive and heart failure patients. Targeting a basolateral membrane protein could provide therapeutic advantages over conventional diuretics. For example, loop (furosemide and bumetanide) and

Molecular Pharmacology Fast Forward. Published on June 12, 2018 as DOI: 10.1124/mol.118.112359
This article has not been copyedited and formatted. The final version may differ from this version.

thiazide diuretics must be secreted into the tubule fluid before reaching their respective luminal target sites in the TAL and DCT (Hasannejad et al., 2004; Hasegawa et al., 2007; Uwai et al., 2000; Vallon et al., 2008). In clinical settings where diuretic secretion is compromised, such as chronic kidney disease or when other drugs compete for renal tubule secretion, the availability of a diuretic that acts basolaterally and independently of renal secretion would be beneficial over conventional diuretics. Furthermore, a recent study by Rao and colleagues demonstrated that a majority of loop diuretic resistance cases in their heart failure patient cohort resulted from enhanced distal tubule Na^+ reabsorption. The authors suggested that administration of thiazide diuretics or a combination of thiazide and K^+-sparing diuretics should help overcome loop diuretic resistance in some patients (Rao et al., 2017). An inhibitor of Kir4.1-containing channels would be potentially superior to thiazide or K^+-sparing diuretics because it would simultaneously inhibit Na^+ reabsorption all along the nephron without sparing K^+. The development of VU0134992 provides the first *in vivo*-active tool compound to enable these and other hypotheses to be tested.

Molecular Pharmacology Fast Forward. Published on June 12, 2018 as DOI: 10.1124/mol.118.112359
This article has not been copyedited and formatted. The final version may differ from this version.

AUTHOR CONTRIBUTIONS

Research Design: SVK, HK, ALB, EF, AD, LMS, JM, CWL, CDW, CRH, JSD

Conducted experiments: SVK, HK, ALB, EF, AD, MK, ED, PV, DF

Performed data analysis: SVK, HK, ALB, EF, AD, MK, ED, DF

Contributed new reagents or analytical tools: HK, AMB, JM, CRH

Wrote manuscript: SVK, HK, ALB, EF, PV, AD, CDW, CWL, CRH, JSD

Molecular Pharmacology Fast Forward. Published on June 12, 2018 as DOI: 10.1124/mol.118.112359
This article has not been copyedited and formatted. The final version may differ from this version.

REFERENCES

Arechiga-Figueroa IA, Marmolejo-Murillo LG, Cui M, Delgado-Ramirez M, van der Heyden MAG, Sanchez-Chapula JA and Rodriguez-Menchaca AA (2017) High-potency block of Kir4.1 channels by pentamidine: Molecular basis. *Eur J Pharmacol* **815**: 56-63.

Barth P, Schonbrun J and Baker D (2007) Toward high-resolution prediction and design of transmembrane helical protein structures. *Proc Natl Acad Sci U S A* **104**(40): 15682-15687.

Bhave G, Chauder BA, Liu W, Dawson ES, Kadakia R, Nguyen TT, Lewis LM, Meiler J, Weaver CD, Satlin LM, Lindsley CW and Denton JS (2011) Development of a selective small-molecule inhibitor of Kir1.1, the renal outer medullary potassium channel. *Mol Pharmacol* **79**(1): 42-50.

Bockenhauer D, Feather S, Stanescu HC, Bandulik S, Zdebik AA, Reichold M, Tobin J, Lieberer E, Sterner C, Landoure G, Arora R, Sirimanna T, Thompson D, Cross JH, van't Hoff W, Al Masri O, Tullus K, Yeung S, Anikster Y, Klootwijk E, Hubank M, Dillon MJ, Heitzmann D, Arcos-Burgos M, Knepper MA, Dobbie A, Gahl WA, Warth R, Sheridan E and Kleta R (2009) Epilepsy, ataxia, sensorineural deafness, tubulopathy, and *KCNJ10* mutations. *N Engl J Med* **360**(19): 1960-1970.

Denton JS, Pao AC and Maduke M (2013) Invited Review - Novel Diuretic Targets. *Am J Physiol Renal Physiol* **305**(7): F931-942.

Djukic B, Casper KB, Philpot BD, Chin LS and McCarthy KD (2007) Conditional knock-out of Kir4.1 leads to glial membrane depolarization, inhibition of potassium and glutamate uptake, and enhanced short-term synaptic potentiation. *J Neurosci* **27**(42): 11354-11365.

Fan L, Wang X, Zhang D, Duan X, Zhao C, Zu M, Meng X, Zhang C, Su XT, Wang MX, Wang WH and Gu R (2015) Vasopressin-induced stimulation of the Na^+-activated K^+ channels is responsible for maintaining the basolateral K^+ conductance of the thick ascending limb (TAL) in EAST/SeSAME syndrome. *Biochim Biophys Acta* **1852**(11): 2554-2562.

Furutani K, Ohno Y, Inanobe A, Hibino H and Kurachi Y (2009) Mutational and in silico analyses for antidepressant block of astroglial inward-rectifier Kir4.1 channel. *Mol Pharmacol* **75**(6): 1287-1295.

Garcia ML, Priest BT, Alonso-Galicia M, Zhou X, Felix JP, Brochu RM, Bailey T, Thomas-Fowlkes B, Liu J, Swensen A, Pai LY, Xiao J, Hernandez M, Hoagland K, Owens K, Tang H, de Jesus RK, Roy S, Kaczorowski GJ and Pasternak A (2014) Pharmacologic inhibition of the renal outer medullary potassium channel causes diuresis and natriuresis in the absence of kaliuresis. *J Pharmacol Exp Ther* **348**(1): 153-164.

Hasannejad H, Takeda M, Taki K, Shin HJ, Babu E, Jutabha P, Khamdang S, Aleboyeh M, Onozato ML, Tojo A, Enomoto A, Anzai N, Narikawa S, Huang XL, Niwa T and Endou H (2004) Interactions of human organic anion transporters with diuretics. *J Pharmacol Exp Ther* **308**(3): 1021-1029.

Hasegawa M, Kusuhara H, Adachi M, Schuetz JD, Takeuchi K and Sugiyama Y (2007) Multidrug resistance-associated protein 4 is involved in the urinary excretion of hydrochlorothiazide and furosemide. *J Am Soc Nephrol* **18**(1): 37-45.

Hibino H, Inanobe A, Furutani K, Murakami S, Findlay I and Kurachi Y (2010) Inwardly rectifying potassium channels: their structure, function, and physiological roles. *Physiol Rev* **90**(1): 291-366.

Kahanovitch U, Cuddapah VA, Pacheco NL, Holt LM, Mulkey DK, Percy AK and Olsen ML (2018) MeCP2 Deficiency Leads to Loss of Glial Kir4.1. *eNeuro* **5**(1).

Kharade S, Sheehan J, Figueroa E, Meiler J and Denton J (2017) Pore polarity and charge determine differential block of Kir1.1 and Kir7.1 potassium channels by the small-molecule inhibitor VU590. *Mol Pharmacol*.

Kharade SV, Flores D, Lindsley CW, Satlin LM and Denton JS (2015) ROMK Inhibitor Actions in the Nephron Probed with Diuretics. *Am J Physiol Renal Physiol*: ajprenal 00423 02015.

King NP, Sheffler W, Sawaya MR, Vollmar BS, Sumida JP, Andre I, Gonen T, Yeates TO and Baker D (2012) Computational design of self-assembling protein nanomaterials with atomic level accuracy. *Science* **336**(6085): 1171-1174.

Kofuji P, Biedermann B, Siddharthan V, Raap M, Iandiev I, Milenkovic I, Thomzig A, Veh RW, Bringmann A and Reichenbach A (2002) Kir potassium channel subunit expression in retinal glial cells: implications for spatial potassium buffering. *Glia* **39**(3): 292-303.

Kothiwale S, Mendenhall JL and Meiler J (2015) BCL::Conf: small molecule conformational sampling using a knowledge based rotamer library. *J Cheminform* **7**: 47.

Kucheryavykh YV, Kucheryavykh LY, Nichols CG, Maldonado HM, Baksi K, Reichenbach A, Skatchkov SN and Eaton MJ (2007) Downregulation of Kir4.1 inward rectifying potassium channel subunits by RNAi impairs potassium transfer and glutamate uptake by cultured cortical astrocytes. *Glia* **55**(3): 274-281.

Lachheb S, Cluzeaud F, Bens M, Genete M, Hibino H, Lourdel S, Kurachi Y, Vandewalle A, Teulon J and Paulais M (2008) Kir4.1/Kir5.1 channel forms the major K^+ channel in the basolateral membrane of mouse renal collecting duct principal cells. *Am J Physiol Renal Physiol* **294**(6): F1398-1407.

Leaver-Fay A, Tyka M, Lewis SM, Lange OF, Thompson J, Jacak R, Kaufman K, Renfrew PD, Smith CA, Sheffler W, Davis IW, Cooper S, Treuille A, Mandell DJ, Richter F, Ban YE, Fleishman SJ, Corn JE, Kim DE, Lyskov S, Berrondo M, Mentzer S, Popovic Z, Havranek JJ, Karanicolas J, Das R, Meiler J, Kortemme T, Gray JJ, Kuhlman B, Baker D and Bradley P (2007) ROSETTA3: an object-oriented software suite for the simulation and design of macromolecules. *Methods Enzymol* **487**: 545-574.

Lewis LM, Bhave G, Chauder BA, Banerjee S, Lornsen KA, Redha R, Fallen K, Lindsley CW, Weaver CD and Denton JS (2009) High-throughput screening reveals a small-molecule inhibitor of the renal outer medullary potassium channel and Kir7.1. *Mol Pharmacol* **76**(5): 1094-1103.

Liu W, Morimoto T, Woda C, Kleyman TR and Satlin LM (2007) Ca^{2+} dependence of flow-stimulated K^+ secretion in the mammalian cortical collecting duct. *Am J Physiol Renal Physiol* **293**(1): F227-235.

Liu W, Wei Y, Sun P, Wang WH, Kleyman TR and Satlin LM (2009) Mechanoregulation of BK channel activity in the mammalian cortical collecting duct: role of protein kinases A and C. *Am J Physiol Renal Physiol* **297**(4): F904-915.

Lourdel S, Paulais M, Cluzeaud F, Bens M, Tanemoto M, Kurachi Y, Vandewalle A and Teulon J (2002) An inward rectifier K^+ channel at the basolateral membrane of the mouse distal convoluted tubule: similarities with Kir4-Kir5.1 heteromeric channels. *J Physiol* **538**(Pt 2): 391-404.

Mandell DJ, Coutsias EA and Kortemme T (2009) Sub-angstrom accuracy in protein loop reconstruction by robotics-inspired conformational sampling. *Nat Methods* **6**(8): 551-552.

Marmolejo-Murillo LG, Arechiga-Figueroa IA, Cui M, Moreno-Galindo EG, Navarro-Polanco RA, Sanchez-Chapula JA, Ferrer T and Rodriguez-Menchaca AA (2017a) Inhibition of Kir4.1 potassium channels by quinacrine. *Brain Res* **1663**: 87-94.

Marmolejo-Murillo LG, Arechiga-Figueroa IA, Moreno-Galindo EG, Navarro-Polanco RA, Rodriguez-Menchaca AA, Cui M, Sanchez-Chapula JA and Ferrer T (2017b) Chloroquine blocks the Kir4.1 channels by an open-pore blocking mechanism. *Eur J Pharmacol* **800**: 40-47.

Meiler J and Baker D (2006) ROSETTALIGAND: protein-small molecule docking with full side-chain flexibility. *Proteins* **65**(3): 538-548.

Nwaobi SE, Cuddapah VA, Patterson KC, Randolph AC and Olsen ML (2016) The role of glial-specific Kir4.1 in normal and pathological states of the CNS. *Acta Neuropathol* **132**(1): 1-21.

Ohno Y, Hibino H, Lossin C, Inanobe A and Kurachi Y (2007) Inhibition of astroglial Kir4.1 channels by selective serotonin reuptake inhibitors. *Brain Res* **1178**: 44-51.

Olsen ML and Sontheimer H (2008) Functional implications for Kir4.1 channels in glial biology: from K^+ buffering to cell differentiation. *J Neurochem* **107**(3): 589-601.

Paulais M, Bloch-Faure M, Picard N, Jacques T, Ramakrishnan SK, Keck M, Sohet F, Eladari D, Houillier P, Lourdel S, Teulon J and Tucker SJ (2011) Renal phenotype in mice lacking the Kir5.1 (*KCNJ16*) K^+ channel subunit contrasts with that observed in SeSAME/EAST syndrome. *Proc Natl Acad Sci U S A* **108**(25): 10361-10366.

Pearson WL, Skatchkov SN, Eaton MJ and Nichols CG (2006) C-terminal determinants of Kir4.2 channel expression. *J Membr Biol* **213**(3): 187-193.

Penton D, Czogalla J, Wengi A, Himmerkus N, Loffing-Cueni D, Carrel M, Rajaram RD, Staub O, Bleich M, Schweda F and Loffing J (2016) Extracellular K^+ rapidly controls NaCl cotransporter phosphorylation in the native distal convoluted tubule by Cl^--dependent and independent mechanisms. *J Physiol* **594**(21): 6319-6331.

Pessia M, Imbrici P, D'Adamo MC, Salvatore L and Tucker SJ (2001) Differential pH sensitivity of Kir4.1 and Kir4.2 potassium channels and their modulation by heteropolymerisation with Kir5.1. *J Physiol* **532**(Pt 2): 359-367.

Rao VS, Planavsky N, Hanberg JS, Ahmad T, Brisco-Bacik MA, Wilson FP, Jacoby D, Chen M, Tang WHW, Cherney DZI, Ellison DH and Testani JM (2017) Compensatory Distal Reabsorption Drives Diuretic Resistance in Human Heart Failure. *J Am Soc Nephrol* **28**(11): 3414-3424.

Raphemot R, Kadakia RJ, Olsen ML, Banerjee S, Days E, Smith SS, Weaver CD and Denton JS (2013) Development and validation of fluorescence-based and automated patch clamp-based functional

assays for the inward rectifier potassium channel Kir4.1. *Assay Drug Dev Technol* **11**(9-10): 532-543.

Raphemot R, Lonergan DF, Nguyen TT, Utley T, Lewis LM, Kadakia R, Weaver CD, Gogliotti R, Hopkins C, Lindsley CW and Denton JS (2011) Discovery, characterization, and structure-activity relationships of an inhibitor of inward rectifier potassium (Kir) channels with preference for kir2.3, kir3.x, and kir7.1. *Front Pharmacol* **2**: 75.

Raphemot R, Swale DR, Dadi PK, Jacobson DA, Cooper P, Wojtovich AP, Banerjee S, Nichols C and Denton JS (2014) Direct Activation of beta-cell K_{ATP} Channels with a Novel Xanthine Derivative. *Mol Pharmacol.*

Reichold M, Zdebik AA, Lieberer E, Rapedius M, Schmidt K, Bandulik S, Sterner C, Tegtmeier I, Penton D, Baukrowitz T, Hulton SA, Witzgall R, Ben-Zeev B, Howie AJ, Kleta R, Bockenhauer D and Warth R (2010) *KCNJ10* gene mutations causing EAST syndrome (epilepsy, ataxia, sensorineural deafness, and tubulopathy) disrupt channel function. *Proc Natl Acad Sci U S A* **107**(32): 14490-14495.

Scholl UI, Choi M, Liu T, Ramaekers VT, Hausler MG, Grimmer J, Tobe SW, Farhi A, Nelson-Williams C and Lifton RP (2009) Seizures, sensorineural deafness, ataxia, mental retardation, and electrolyte imbalance (SeSAME syndrome) caused by mutations in *KCNJ10*. *Proc Natl Acad Sci U S A* **106**(14): 5842-5847.

Sicca F, Ambrosini E, Marchese M, Sforna L, Servettini I, Valvo G, Brignone MS, Lanciotti A, Moro F, Grottesi A, Catacuzzeno L, Baldini S, Hasan S, D'Adamo MC, Franciolini F, Molinari P, Santorelli FM and Pessia M (2016) Gain-of-function defects of astrocytic Kir4.1 channels in children with autism spectrum disorders and epilepsy. *Sci Rep* **6**: 34325.

Sicca F, Imbrici P, D'Adamo MC, Moro F, Bonatti F, Brovedani P, Grottesi A, Guerrini R, Masi G, Santorelli FM and Pessia M (2011) Autism with seizures and intellectual disability: possible

causative role of gain-of-function of the inwardly-rectifying K+ channel Kir4.1. *Neurobiol Dis* **43**(1): 239-247.

Su S, Ohno Y, Lossin C, Hibino H, Inanobe A and Kurachi Y (2007) Inhibition of astroglial inwardly rectifying Kir4.1 channels by a tricyclic antidepressant, nortriptyline. *J Pharmacol Exp Ther* **320**(2): 573-580.

Su XT and Wang WH (2016) The expression, regulation, and function of Kir4.1 (*KCNJ10*) in the mammalian kidney. *Am J Physiol Renal Physiol* **311**(1): F12-15.

Swale DR, Kharade SV and Denton JS (2014) Cardiac and renal inward rectifier potassium channel pharmacology: emerging tools for integrative physiology and therapeutics. *Curr Opin Pharmacol* **15**: 7-15.

Swale DR, Kurata H, Kharade SV, Sheehan J, Raphemot R, Voigtritter KR, Figueroa EE, Meiler J, Blobaum AL, Lindsley CW, Hopkins CR and Denton JS (2016) ML418: The First Selective, Sub-Micromolar Pore Blocker of Kir7.1 Potassium Channels. *ACS Chem Neurosci* **7**(7): 1013-1023.

Takanari H, Nalos L, Stary-Weinzinger A, de Git KC, Varkevisser R, Linder T, Houtman MJ, Peschar M, de Boer TP, Tidwell RR, Rook MB, Vos MA and van der Heyden MA (2013) Efficient and specific cardiac IK_1 inhibition by a new pentamidine analogue. *Cardiovasc Res* **99**(1): 203-214.

Tong X, Ao Y, Faas GC, Nwaobi SE, Xu J, Haustein MD, Anderson MA, Mody I, Olsen ML, Sofroniew MV and Khakh BS (2014) Astrocyte Kir4.1 ion channel deficits contribute to neuronal dysfunction in Huntington's disease model mice. *Nat Neurosci* **17**(5): 694-703.

Tucker SJ, Imbrici P, Salvatore L, D'Adamo MC and Pessia M (2000) pH dependence of the inwardly rectifying potassium channel, Kir5.1, and localization in renal tubular epithelia. *J Biol Chem* **275**(22): 16404-16407.

Uwai Y, Saito H, Hashimoto Y and Inui KI (2000) Interaction and transport of thiazide diuretics, loop diuretics, and acetazolamide via rat renal organic anion transporter rOAT1. *J Pharmacol Exp Ther* **295**(1): 261-265.

Vallon V, Rieg T, Ahn SY, Wu W, Eraly SA and Nigam SK (2008) Overlapping in vitro and in vivo specificities of the organic anion transporters OAT1 and OAT3 for loop and thiazide diuretics. *Am J Physiol Renal Physiol* **294**(4): F867-873.

Welling PA (2016) Roles and Regulation of Renal K Channels. *Annu Rev Physiol* **78**: 415-435.

Zaika O, Mamenko M, Palygin O, Boukelmoune N, Staruschenko A and Pochynyuk O (2013a) Direct inhibition of basolateral Kir4.1/5.1 and Kir4.1 channels in the cortical collecting duct by dopamine. *Am J Physiol Renal Physiol* **305**(9): F1277-1287.

Zaika OL, Mamenko M, Palygin O, Boukelmoune N, Staruschenko A and Pochynyuk O (2013b) Direct inhibition of basolateral Kir4.1/5.1 and Kir4.1 channels in the cortical collecting duct by dopamine. *Am J Physiol Renal Physiol* **305**(9): F1277-1287.

Zhang C, Wang L, Su XT, Lin DH and Wang WH (2015) KCNJ10 (Kir4.1) is expressed in the basolateral membrane of the cortical thick ascending limb. *Am J Physiol Renal Physiol* **308**(11): F1288-1296.

Zhang C, Wang L, Thomas S, Wang K, Lin DH, Rinehart J and Wang WH (2013) Src family protein tyrosine kinase regulates the basolateral K channel in the distal convoluted tubule (DCT) by phosphorylation of KCNJ10 protein. *J Biol Chem* **288**(36): 26135-26146.

Zhang C, Wang L, Zhang J, Su XT, Lin DH, Scholl UI, Giebisch G, Lifton RP and Wang WH (2014) *KCNJ10* determines the expression of the apical Na-Cl cotransporter (NCC) in the early distal convoluted tubule (DCT1). *Proc Natl Acad Sci U S A* **111**(32): 11864-11869.

Zhang X, Su J, Cui N, Gai H, Wu Z and Jiang C (2011) The disruption of central CO_2 chemosensitivity in a mouse model of Rett syndrome. *Am J Physiol Cell Physiol* **301**(3): C729-738.

Zhou X, Forrest MJ, Sharif-Rodriguez W, Forrest G, Szeto D, Urosevic-Price O, Zhu Y, Stevenson AS, Zhou Y, Stribling S, Dajee M, Walsh SP, Pasternak A and Sullivan KA (2017) Chronic Inhibition of Renal Outer Medullary Potassium Channel Not Only Prevented but Also Reversed Development of Hypertension and End-Organ Damage in Dahl Salt-Sensitive Rats. *Hypertension* **69**(2): 332-338.

Molecular Pharmacology Fast Forward. Published on June 12, 2018 as DOI: 10.1124/mol.118.112359
This article has not been copyedited and formatted. The final version may differ from this version.

FOOTNOTES

Work in the Denton laboratory was funded by National Institutes of Health grants [5R21 NS073097-01S1and R01DK082884]. E.F. was supported by National Institutes of Health Training grant [5 T32 GM007628]. Work in the Meiler laboratory is supported by National Institutes of Health Grants [R01 GM080403, R01 HL122010] and National Science Foundation grant [CHE 1305874]. Work in the Satlin laboratory is supported through National Institutes of Health grants [DK038470 and P30 DK079307, The Pittsburgh Center for Kidney Research]. The WaveFront Biosciences Panoptic kinetic imaging plate reader is housed and managed within the Vanderbilt High-throughput Screening Core Facility, an institutionally supported core, and was funded by National Institutes of Health Shared Instrumentation Grant [1S10OD021734]. All authors other than CDW declare they have no conflicts of interest. CDW is an owner of WaveFront Biosciences, manufacturer of the Panoptic plate reader. CDW receives royalties from the sales of Thallos via a licensing agreement with Vanderbilt University.

Molecular Pharmacology Fast Forward. Published on June 12, 2018 as DOI: 10.1124/mol.118.112359
This article has not been copyedited and formatted. The final version may differ from this version.

FIGURE LEGENDS

Figure 1: VU0134992 exhibits preference for Kir4.1 over Kir4.1-5.1 channels. A. Chemical structure of VU0134992. **B.** Representative traces showing inhibition of Kir4.1 homomeric and Kir4.1-5.1 heteromeric currents recorded in absence (blue) or in presence of 3 μM VU0134992 (red) and 2 mM $BaCl_2$ (black). **C.** Mean ± SD CRCs of VU0134992 for homotetrameric Kir4.1 and heterotetrameric concatemer of Kir4.1/5.1 currents measured at -120 mV ($n \geq 5$). **D.** Mean ± SD CRCs of VU0134992 for homotetrameric Kir4.1 and heterotetrameric concatemer of Kir4.1/5.1 currents measured at +120 mV ($n \geq 5$).

Figure 2: VU0134992 exhibits voltage-dependent block of Kir4.1 A. Representative whole-cell current responses to voltage steps (1 s) from a holding potentials (-80 mV for $5K^+$ or -25 mV for $50K^+$) in presence or absence of 30 μM VU0134992. **B.** Percent VU0134992 inhibition was calculated at each voltage with 5 and 50 mM extracellular K^+. The VU0134992 induced block of Kir4.1 was statistically significantly lower at -120 mV and -100 mV in 50 mM K^+ as compared to 5 mM K^+ containing bath solution. *$P < 0.05$, statistically significantly different from the 5 mM K^+ extracellular solution control ($n \geq 5$).

Figure 3: E158 and I159 are required for effective block of Kir4.1 by VU0134992. A. (Left) Kir4.1 homology model showing the location of E158 (green), which is it predicted to interact with VU0134992. (Right) magnified section of the Kir4.1 homology model (red square in left) showing interaction of VU0134992 with the pore lining E158 residue in Kir4.1. **B.** Mutagenesis studies were carried out to test the prediction of homology model. Bar graph showing percent inhibition of Kir4.1-WT (solid grey bar), and various mutant channels (colored or open bars) at 3 μM VU0134992. Kir4.1 carrying mutations at E158 and I159 residue showed statistically significantly reduced sensitivity to VU0134992. **C.** Representative traces showing inhibition of WT and E158N/Q/D and I159S mutants in

Molecular Pharmacology Fast Forward. Published on June 12, 2018 as DOI: 10.1124/mol.118.112359
This article has not been copyedited and formatted. The final version may differ from this version.

absence (blue) or in presence of 3 μM VU0134992 (red) and 2 mM $BaCl_2$ (black). **D.** VU0134992 CRCs comparing Kir4.1-WT, Kir1.1 and Kir4.1-E158N, E158D, E158Q and I159S mutants at -120 mV. **E.** CRCs for indicated channels measured at +120 mV. *P < 0.05, statistically significantly different from the WT control (n≥5).

Figure 4. Overview of VU0134992 SAR. Inhibition of Tl^+ flux toward Kir4.1 was evaluated for each compound synthesized according to Figures S1-S3. Specific figures of IC_{50} are described in Tables S1-S3.

Figure 5. Dose-dependent effects of VU0134992 on renal excretion. Rats were given oral gavage of either vehicle alone or the indicated doses of VU0134992 followed by saline volume load and were placed in metabolic cages for collection of urine over a 4 h period. VU0134992 statistically significantly (P<0.05) increased **A.** urine volume, **B.** urine Na^+, and **C.** urine K^+ at doses of 50 mg/kg and 100 mg/kg as compared to the vehicle control. *P < 0.05, statistically significantly different from the vehicle control (n≥4).

Figure 6. Regulation of renal ion transport by Kir4.1. In the TAL (left panel), heteromeric Kir4.1/5.1 channels recycle K^+ across the basolateral membrane to maintain the activity of the Na^+/K^+-ATPase, which creates a favorable gradient for Na^+ and K^+ uptake via NKCC2. Kir4.1/5.1 is functionally coupled to basolateral ClC-Kb channels through unknown mechanisms. Inhibition of Kir4.1 should reduce Na^+, Cl^-, and K^+ reabsorption in the TAL. In the DCT (middle panel), basolateral K^+ secretion via Kir4.1/5.1 energizes the Na^+/K^+-ATPase to maintain a favorable chemical driving force for Na+ uptake by NCC. Kir4.1/5.1 also regulates the basolateral membrane potential and is functionally coupled to ClC-Kb. Inhibition of Kir4.1/5.1 should increase intracellular Cl^- concentration and inhibit NCC function via the WNK-SPAK kinase pathway (not shown; see Discussion). In the CCD (right panel), homomeric Kir4.1 and heteromeric Kir4.1/5.1 channels hyperpolarize the basolateral membrane potential and electrically

Molecular Pharmacology Fast Forward. Published on June 12, 2018 as DOI: 10.1124/mol.118.112359
This article has not been copyedited and formatted. The final version may differ from this version.

coupled apical membrane potential and promote luminal Na^+ reabsorption by ENaC. Inhibition of Kir4.1 or Kir4.1/5.1 channels in the CCD should depolarize the membrane potential and reduce the electrochemical driving force for Na^+ reabsorption.

Molecular Pharmacology Fast Forward. Published on June 12, 2018 as DOI: 10.1124/mol.118.112359
This article has not been copyedited and formatted. The final version may differ from this version.

TABLES

Table 1. Comparison of VU0134992 and antidepressant selectivity for Kir4.1 over other Kir channels. Data shown are mean IC_{50} values in μM and maximal % inhibition at 30 μM and 90 μM in parentheses derived from Tl^+ flux assays. Experiments were performed in triplicate on two separate days.

Channel	VU0134992	Amitriptyline	Nortriptyline	Fluoxetine
Kir1.1	Inactive	33.0 (16%, 58%)	31.0 (6%, 50%)	27.0 (6%, 30%)
Kir2.1	Inactive	35.0 (1%, 36%)	Inactive	10.1 (10%, 86%)
Kir2.2	Inactive	41.7 (2%, 41%)	Inactive	Inactive
Kir2.3	13.2 (73%)	21.3 (53%, 89%)	19.4 (60%, 91%)	7.1 (98%, 100%)
Kir3.1/3.2	2.5 (92%)	13.6 (73%, 91%)	16.1 (65%, 87%)	3.4 (97%, 100%)
Kir3.1/3.4	3.1 (92%)	12.0 (67%, 88%)	15.0 (56%, 80%)	2.4 (94%, 100%)
Kir4.1	5.2 (100%)	89.0 (0%, 66%)	41.7 (10%, 93%)	31.2 (35%, 95%)
Kir4.2	8.1 (100%)	42.7 (0%, 45%)	46.7 (0%, 65%)	20.2 (98%, 99%)
Kir6.2/SUR1	11.4 (12%)	32.2 (4%, 64%)	42.0 (0%, 52%)	64 (4%, 65%)
Kir7.1	34.2 (15%)	22.9 (65%, 89%)	26.0 (50%, 82%)	5.8 (75%, 92%)

Molecular Pharmacology Fast Forward. Published on June 12, 2018 as DOI: 10.1124/mol.118.112359
This article has not been copyedited and formatted. The final version may differ from this version.

Table 2. Published Kir4.1 inhibitors

Compound	Structure	Drug Class	Kir4.1 IC_{50} (μM)	Reference
Fluoxetine	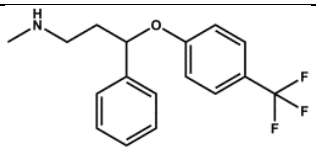	SSRI	15	(Ohno et al., 2007)
Amitriptyline	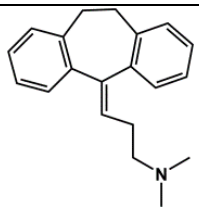	TCA	89	This study
Chloroquine	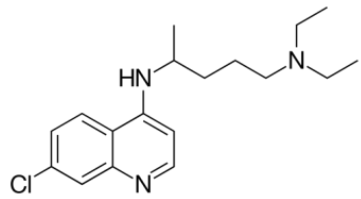	Antimalarial	7	(Marmolejo-Murillo et al., 2017b)
Nortriptyline	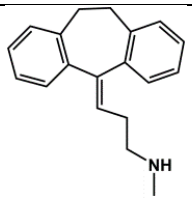	TCA	16-38*	(Su et al., 2007)
Pentamidine	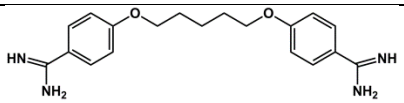	Antimicrobial	0.097**	(Arechiga-Figueroa et al., 2017; Takanari et al., 2013)
Quinacrine	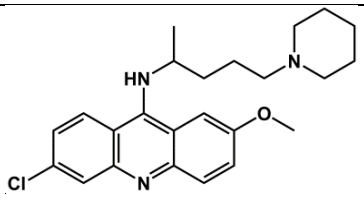	Antimalarial	~3	(Marmolejo-Murillo et al., 2017a)
VU717	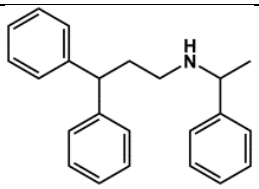	None	6	(Raphemot et al., 2013)

Molecular Pharmacology Fast Forward. Published on June 12, 2018 as DOI: 10.1124/mol.118.112359
This article has not been copyedited and formatted. The final version may differ from this version.

VU0134992	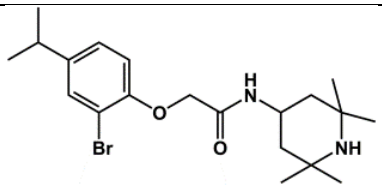	None	0.97	This study

*Voltage-dependent block; calculated at +30 mV and -110 mV, respectively; **voltage-dependent block; calculated at +80 mV in inside-out patch clamp experiments.

Figure 1

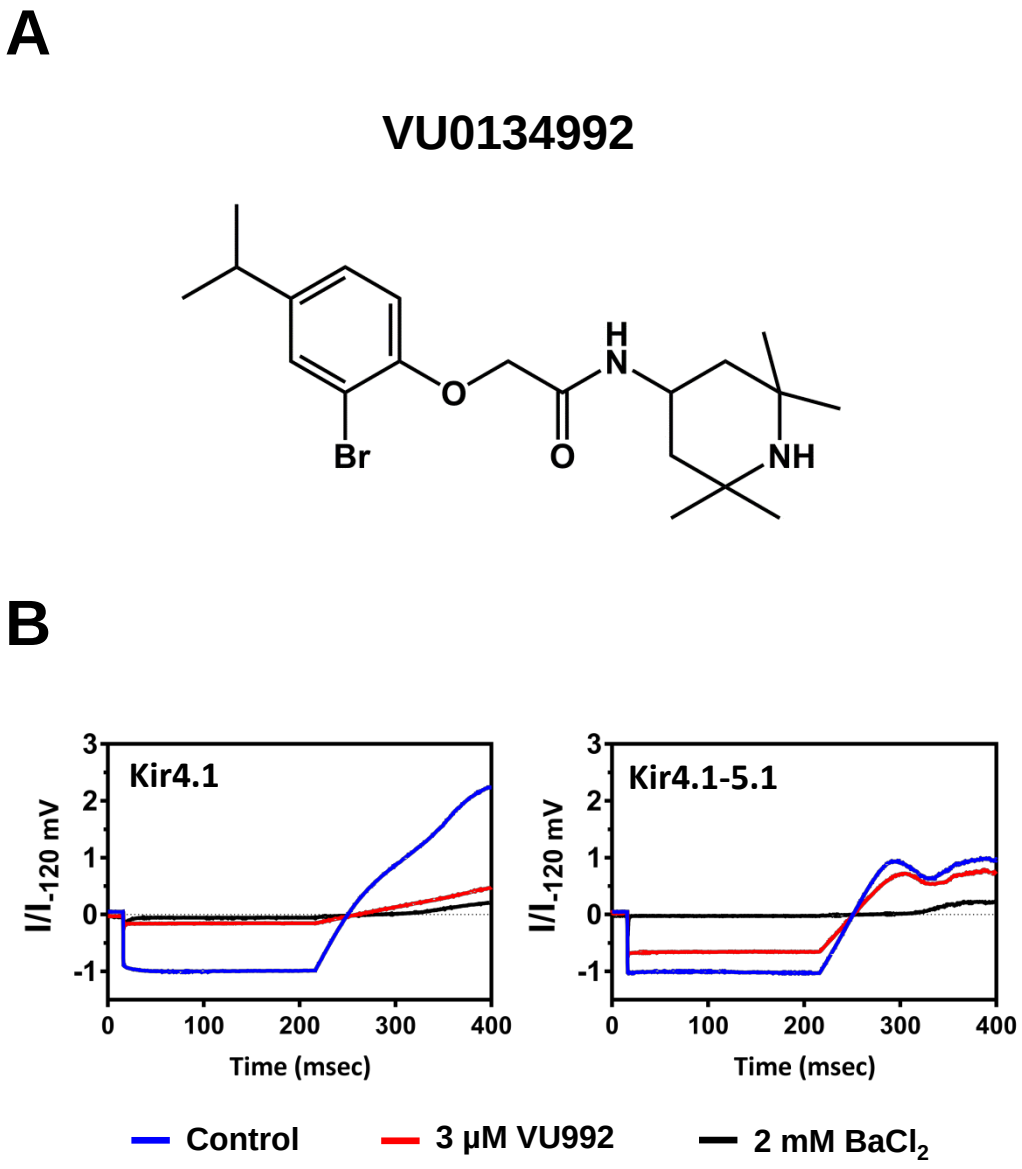

Figure 2

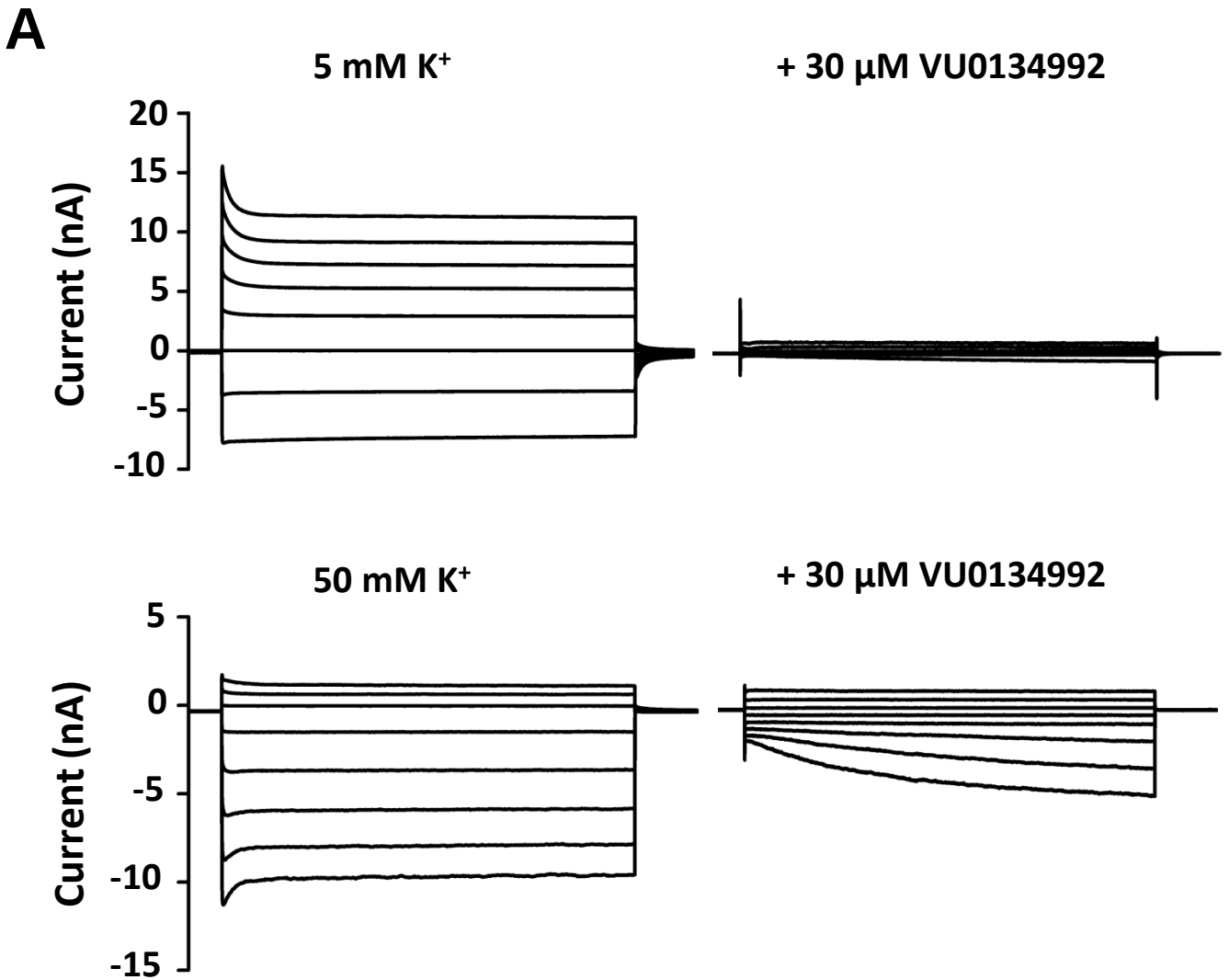

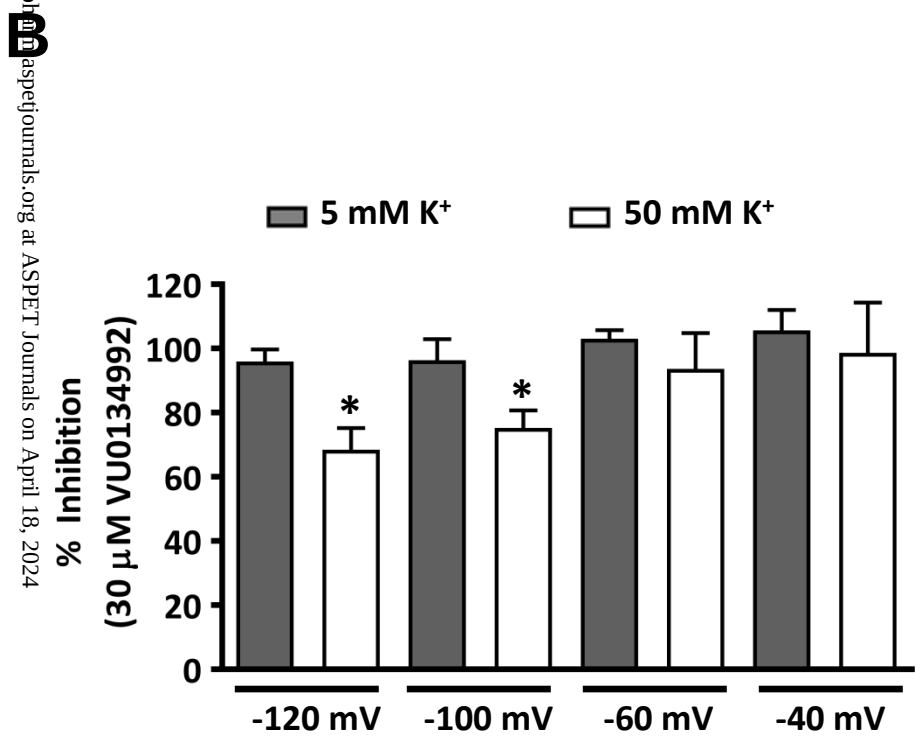

Figure 3

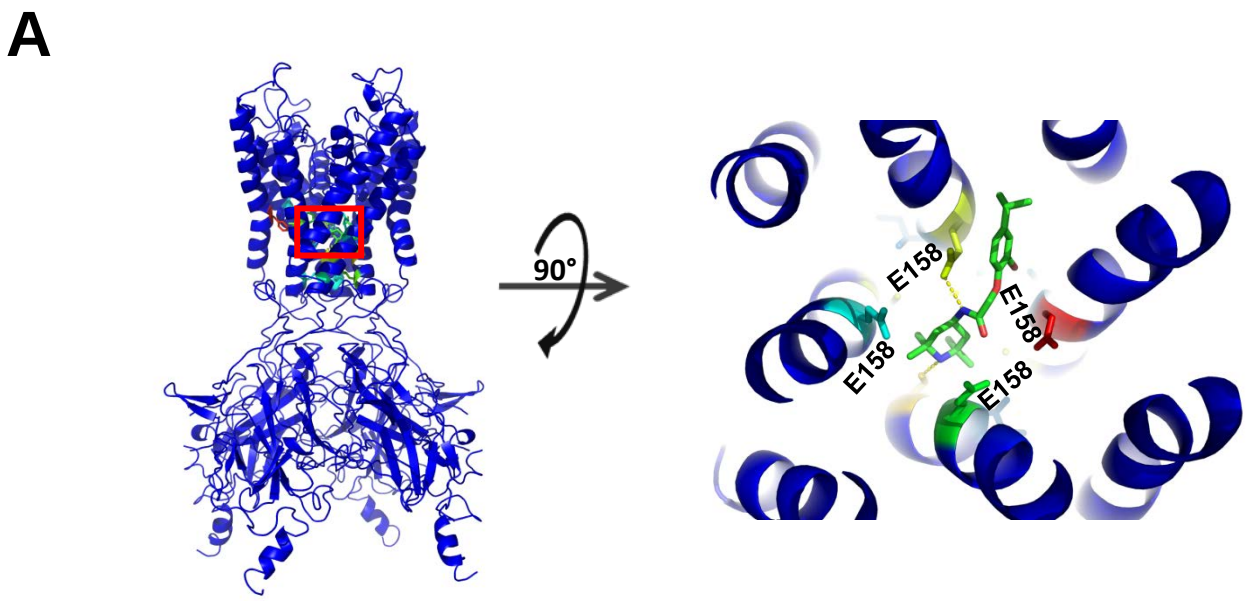

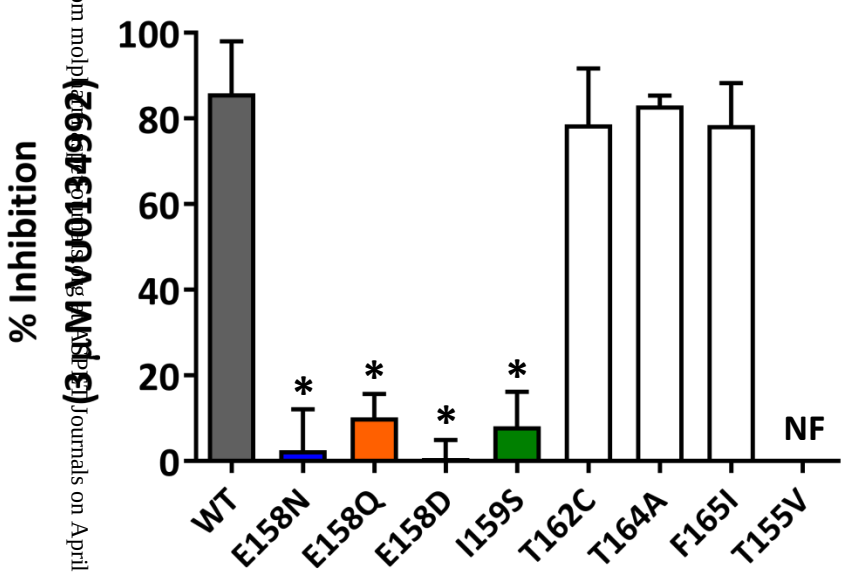

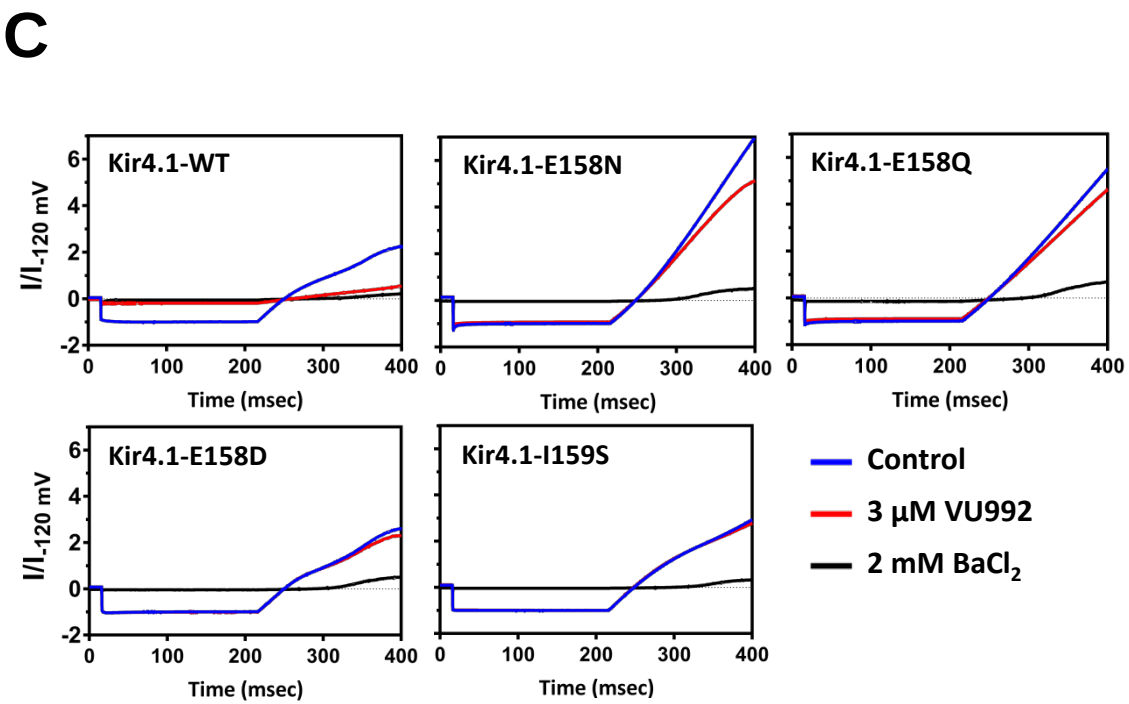

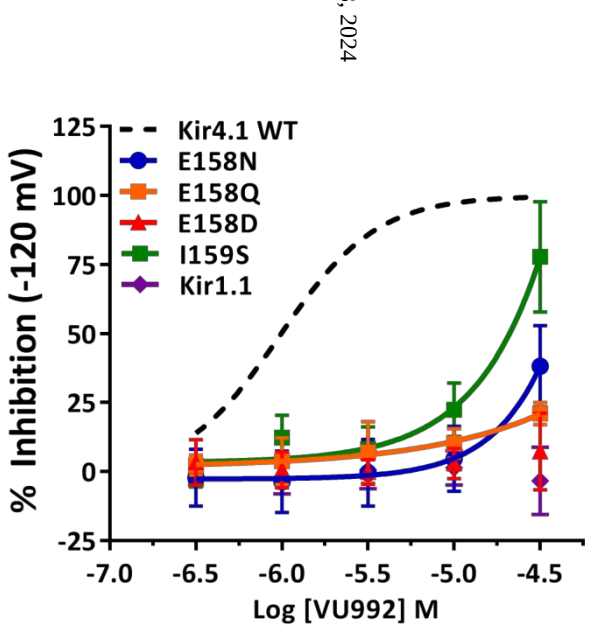

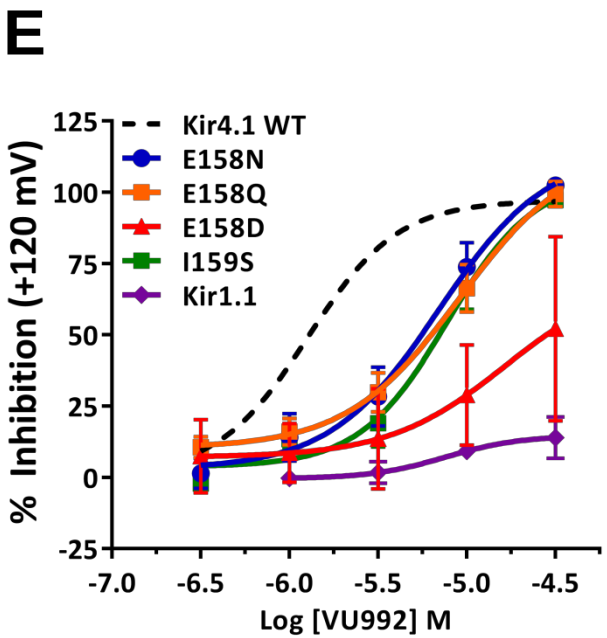

Figure 4

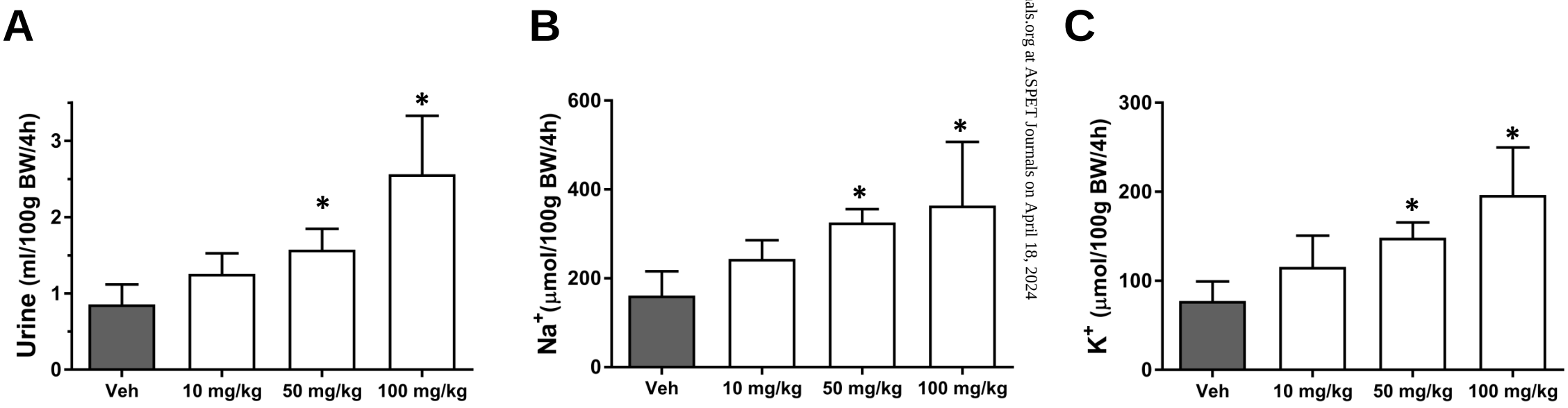

Figure 5

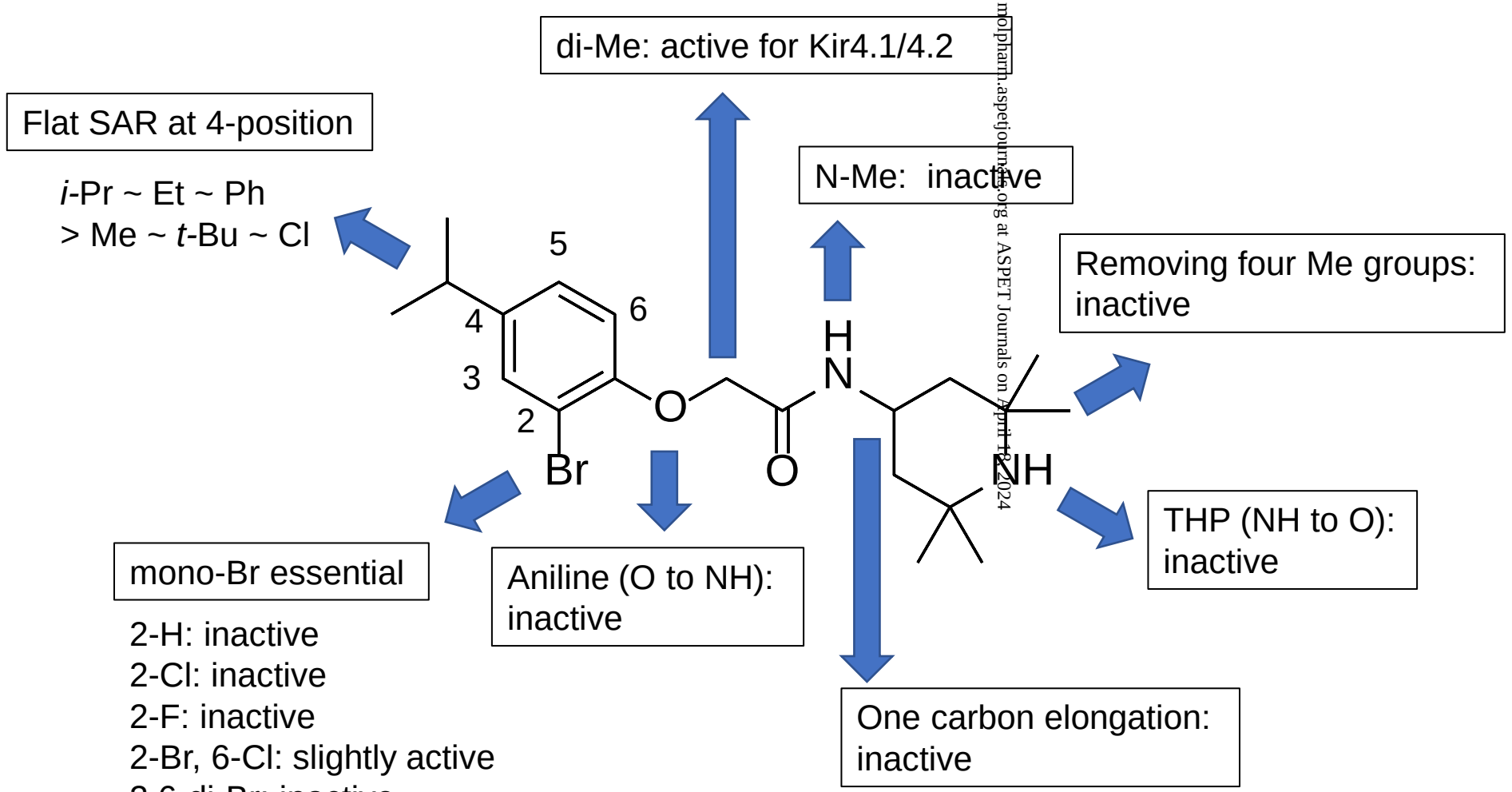

Figure 6

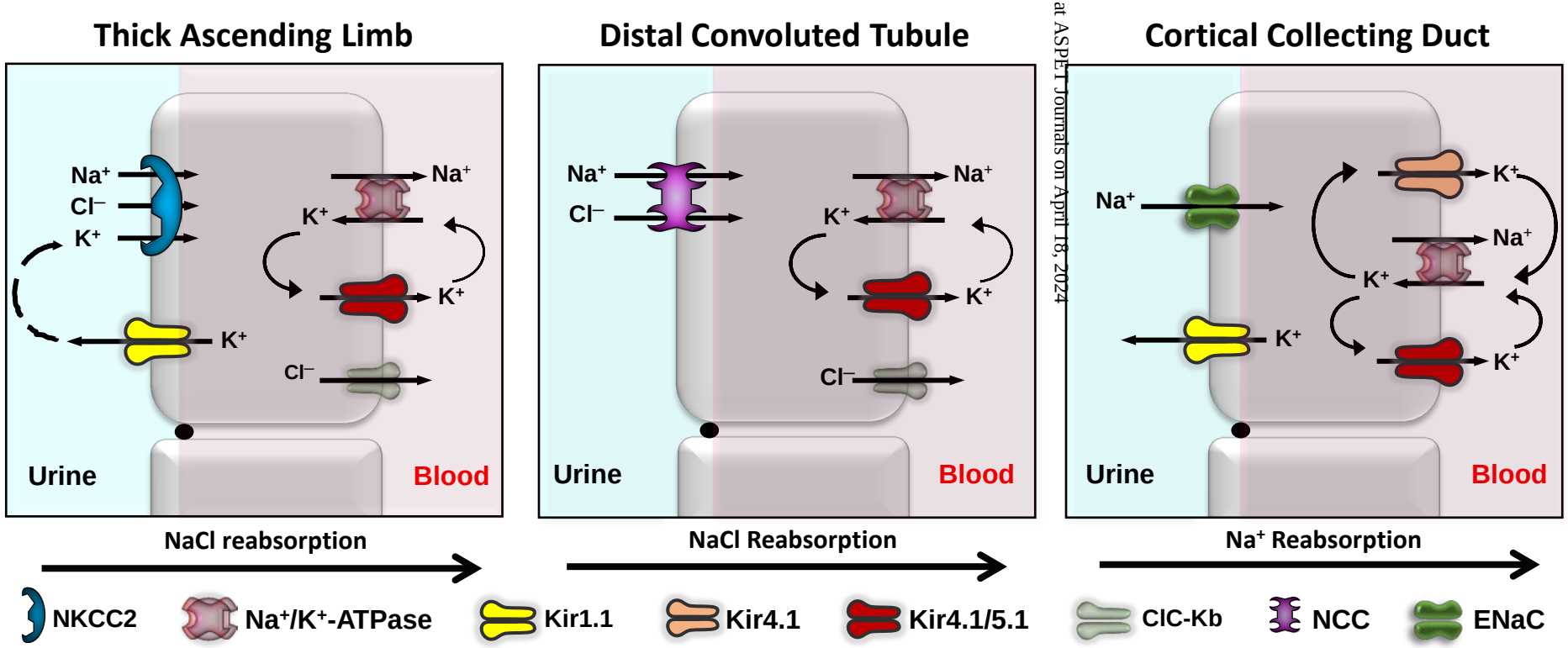

SUPPLEMENTAL INFORMATION

Discovery, characterization, and effects on renal fluid and electrolyte excretion of the Kir4.1 potassium channel pore blocker, VU0134992

Sujay V. Kharade, Haruto Kurata, Aaron M. Bender, Anna L. Blobaum, Eric Figueroa, Amanda Duran, Meghan Kramer, Emily Days, Paige Vinson, Daniel Flores, Lisa M. Satlin, Jens Meiler, C. David Weaver, Craig W. Lindsley, Corey R. Hopkins and Jerod S. Denton

Journal Title: *Molecular Pharmacology*

Supplemental Methods

General Chemical Synthesis

All NMR spectra were recorded on a 400 MHz AMX Bruker NMR spectrometer. ^{1}H and ^{13}C chemical shifts are reported in δ values in ppm downfield with the deuterated solvent as the internal standard. Data are reported as follows: chemical shift, multiplicity (s = singlet, d = doublet, t = triplet, q = quartet, b = broad, m = multiplet), integration, coupling constant (Hz). Low resolution mass spectra were obtained on an Agilent 6120 or 6150 with ESI source. Method A: MS parameters were as follows: fragmentor: 70, capillary voltage: 3000 V, nebulizer pressure: 30 psig, drying gas flow: 13 L/min, drying gas temperature: 350 ºC. Samples were introduced via an Agilent 1290 UHPLC comprised of a G4220A binary pump, G4226A ALS, G1316C TCC, and G4212A DAD with ULD flow cell. UV absorption was generally observed at 215 nm and 254 nm with a 4 nm bandwidth. Column: Waters Acquity BEH C18, 1.0 x 50 mm, 1.7 um. Gradient conditions: 5% to 95% CH_3CN in H_2O (0.1% TFA) over 1.4 min, hold at 95% CH_3CN for 0.1 min, 0.5 mL/min, 55 ºC. Method B: MS parameters were as follows: fragmentor: 100, capillary voltage: 3000 V, nebulizer pressure: 40 psig, drying gas flow: 11 L/min, drying gas temperature: 350 ºC. Samples were introduced via an Agilent 1200 HPLC comprised of a degasser, G1312A binary pump, G1367B HP-ALS, G1316A TCC, G1315D DAD, and a Varian 380 ELSD (if applicable). UV absorption was generally observed at 215 nm and 254 nm with a 4 nm bandwidth. Column: Thermo Accucore C18, 2.1 x 30 mm, 2.6 um. Gradient conditions: 7% to 95%

CH_3CN in H_2O (0.1% TFA) over 1.6 min, hold at 95% CH_3CN for 0.35 min, 1.5 mL/min, 45 ºC. High resolution mass spectra were obtained on an Agilent 6540 UHD Q-TOF with ESI source. MS parameters were as follows: fragmentor: 150, capillary voltage: 3500 V, nebulizer pressure: 60 psig, drying gas flow: 13 L/min, drying gas temperature: 275 ºC. Samples were introduced via an Agilent 1200 UHPLC comprised of a G4220A binary pump, G4226A ALS, G1316C TCC, and G4212A DAD with ULD flow cell. UV absorption was observed at 215 nm and 254 nm with a 4 nm bandwidth. Column: Agilent Zorbax Extend C18, 1.8 µm, 2.1 x 50 mm. Gradient conditions: 5% to 95% CH_3CN in H_2O (0.1% formic acid) over 1 min, hold at 95% CH_3CN for 0.1 min, 0.5 mL/min, 40 ºC. For compounds that were purified on a Gilson preparative reversed-phase HPLC, the system comprised of a 333 aqueous pump with solvent-selection valve, 334 organic pump, GX-271 or GX-281 liquid hander, two column switching valves, and a 155 UV detector. UV wavelength for fraction collection was user-defined, with absorbance at 254 nm always monitored. Method: Phenomenex Axia-packed Luna C18, 30 x 50 mm, 5 µm column. Mobile phase: CH_3CN in H_2O (0.1% TFA). Gradient conditions: 0.75 min equilibration, followed by user defined gradient (starting organic percentage, ending organic percentage, duration), hold at 95% CH_3CN in H_2O (0.1% TFA) for 1 min, 50 mL/min, 23 ºC. Solvents for extraction, washing and chromatography were HPLC grade. All reagents were purchased from Aldrich Chemical Co. and were used without purification.

Intrinsic Clearance in Human and Rat Liver Microsomes

Human or rat liver microsomes (0.5 mg/mL) and 1 µM test compound were incubated in 100 mM potassium phosphate pH 7.4 buffer with 3 mM $MgCl_2$ at 37 ºC with constant shaking. After a 5 min preincubation, the reaction was initiated by addition of NADPH (1 mM). At selected time intervals (0, 3, 7, 15, 25, and 45 min), 50 µL aliquots were taken and subsequently placed into a 96-well plate containing 150 µL of cold acetonitrile with internal standard (50 ng/mL carbamazepine). Plates were

then centrifuged at 3000 rcf (4 ºC) for 10 min, and the supernatant was transferred to a separate 96-well plate and diluted 1:1 with water for LC/MS/MS analysis. The *in vitro* half-life ($T_{1/2}$, min, Eq. 1), intrinsic clearance (CL_{INT}, mL/min/kg, Eq. 2) and subsequent predicted hepatic clearance (CL_{HEP}, mL/min/kg, Eq. 3) were determined employing the following equations:

$$T_{1/2} = \frac{Ln(2)}{k} \quad (1)$$

where k represents the slope from linear regression analysis of the natural log percent remaining of test compound as a function of incubation time

$$CL_{\text{int}} = \frac{0.693}{in\,vitro\,T_{1/2}} x \frac{mL\ incubation}{mg\ microsomes} x \frac{45\,mg\ microsomes}{gram\ liver} x \frac{45^{a}\ gram\ liver}{kg\ body\ wt} \quad (2)$$

[a] scale-up factor of 45 for rat

$$CL_{hep} = \frac{Q_h \cdot CL\,\text{int}}{Q_h + CL\,\text{int}} \quad (3)$$

where Q_h (hepatic blood flow) is 70 mL/min/kg for rat and 21 mL/min/kg for human.

Plasma Protein Binding

The protein binding of each compound was determined in rat or human plasma via equilibrium dialysis employing HTDialysis Teflon dialysis chamber and cellulose membranes (MWCO 12-14 K) (HTDialysis LLC, Gales Ferry, CT). Plasma was added to the 96-well plate containing test compound and mixed thoroughly for a final concentration of 5 µM. Subsequently, 150 µL of the plasma-compound mixture was transferred to the dialysis chamber, with an accompanying 150 µL of phosphate buffer (25 mM, pH 7.4) on the other side of the membrane. The device plate was sealed and incubated for 4 hours at 37 ºC with shaking. At completion, aliquots from each chamber were diluted 1:1 with either plasma (for the buffer sample) or buffer (for the plasma sample) and transferred to a new 96-well plate, at which time ice-cold acetonitrile containing internal standard (50 ng/mL carbamazepine) (2 volumes) was added

to extract the matrices. The plate was centrifuged (3000 rcf, 10 min) and supernatants transferred and diluted 1:1 (supernatant: water) into a new 96 well plate, which was then sealed in preparation for LC/MS/MS analysis. Each compound was assayed in triplicate within the same 96-well plate. Fraction unbound was determined using the following equation:

$$F_u = \frac{Conc_{buffer}}{Conc_{plasma}}$$

Brain Homogenate Binding (rat)

The brain homogenate binding of each compound was determined in rat brain homogenate via equilibrium dialysis employing HTDialysis Teflon dialysis chamber and cellulose membranes (MWCO 12-14 K) (HTDialysis LLC, Gales Ferry, CT). Brain tissue homogenate was prepared by diluting one volume whole rat brain tissue with three volumes of phosphate buffer (25 mM, pH 7.4). The mixture was then subjected to mechanical homogenization employing a Mini-Beadbeater™ and 1.0 mm Zirconia/Silica Beads (BioSpec Products). Brain homogenate spiked with test compound and mixed thoroughly for a final concentration of 5 µM. Subsequently, 150 µL of the brain homogenate-compound mixture was transferred to the dialysis chamber with an accompanying 150 µL of phosphate buffer (25 mM, pH 7.4) on the other side of the membrane. The block was sealed and incubated for 6 hours at 37 ºC with shaking. At completion, aliquots from each side of the chamber were diluted 1:1 with either brain homogenate (to the buffer side) or buffer (to the brain homogenate side) in a new 96 well plate, at which time ice-cold acetonitrile containing internal standard (50 ng/mL carbamazepine) was added to extract the matrices. The plate was centrifuged (3000 rcf, 10 min) and supernatants transferred and diluted 1:1 (supernatant: water) into a new 96 well plate, which was then sealed in preparation for LC/MS/MS analysis. Each compound was assayed in triplicate within the same 96-well plate. Fraction unbound was determined using the following equation:

$$F_{u,tissue} = \frac{1/D_f}{(1/F_{u,\text{hom}} - 1) + 1/D_f}$$

Where $F_{u,hom}$ represent the measured fraction unbound in the diluted homogenate and D_f represents dilution factor.

LC/MS/MS Analysis of Samples from *In Vitro* Assays

Samples were analyzed via electrospray ionization (ESI) on an AB Sciex API-4000 (Foster City, CA) triple-quadrupole instrument that was coupled with Shimadzu LC-10AD pumps (Columbia, MD) and a Leap Technologies CTC PAL auto-sampler (Carrboro, NC). Analytes were separated by gradient elution using a Fortis C18 3.0 x 50 mm, 3 µm column (Fortis Technologies Ltd, Cheshire, UK) thermostated at 40 ºC. HPLC mobile phase A was 0.1% formic acid in water (pH unadjusted), mobile phase B was 0.1% formic acid in acetonitrile (pH unadjusted). The gradient started at 10% B after a 0.2 min hold and was linearly increased to 90% B over 1.2 min; held at 90% B for 0.1 min and returned to 10% B in 0.1 min followed by a re-equilibration (0.9 min). The total run time was 2.5 min and the HPLC flow rate was 0.5 mL/min. The source temperature was set at 500 ºC and mass spectral analyses were performed using multiple reaction monitoring (MRM), with transitions specific for each compound utilizing a Turbo-Ionspray® source in positive ionization mode (5.0 kV spray voltage).

***In-Vivo* PK Methods**

All rodent PK experiments were conducted in accordance with the National Institute of Health regulations of animal care covered in Principles of Laboratory Animal Care (National Institutes of Health publication 85-23, revised 1985) and were approved by the Institutional Animal Care and Use Committee.

Time Course PK and Single Time Point Tissue Distribution Studies

IV cassette PK experiments in rats were carried out according to methods described previously (Bridges et al., 2014). Briefly, a cassette of compounds (n = 4–5/cassette) were formulated from 10 mM solutions of compounds in DMSO. In order to reduce the absolute volume of DMSO that was administered, the compounds were combined and diluted with ethanol and PEG 400 to achieve a final concentration of 0.4–0.5 mg/mL for each compound (2 mg/mL total) administered in each cassette. The final dosing solutions consisted of approximately 10% ethanol, 40% PEG400, and 50% DMSO (v/v). For time course PK studies, each cassette dose was administered IV via the jugular vein to two dual-cannulated (carotid artery and jugular vein) adult male Sprague–Dawley rats, each weighing between 250 and 350 g (Harlan, Indianapolis, IN) for a final dose of 0.2–0.25 mg/kg per compound. Whole blood collections via the carotid artery were performed at 0.033, 0.117, 0.25, 0.5, 1, 2, 4, 7, and 24 hours post dose and plasma samples prepared for bioanalysis. For single time point tissue distribution studies, compounds were formulated as described above (in cassette format) and dosed to male Sprague-Dawley rats for a final dose of 0.2-0.25 mg/kg per compound. Brain dissection and blood collections via the carotid artery were performed 1 hr post dose. The brain samples were rinsed in PBS, snap frozen and stored at -80 °C. Prior to LC/MS/MS analysis, brain samples were thawed to room temperature and subjected to mechanical homogenation employing a Mini-Beadbeater™ and 1.0 mm Zirconia/Silica Beads (BioSpec Products).

Plasma and Brain Sample Preparation

Plasma was separated by centrifugation (4000 rcf, 4 ºC) and stored at –80 ºC until analysis. On the day of analysis, frozen whole brains were weighed and diluted with 1:3 (w/w) parts of 70:30 isopropanol:water. The mixture was then subjected to mechanical homogenization employing a Mini-Beadbeater™ and 1.0 mm Zirconia/Silica Beads (BioSpec Products) followed by centrifugation. The

sample extraction of plasma (20 μL) or brain homogenate (20 μL) was performed by a method based on protein precipitation using three volumes of ice-cold acetonitrile containing an internal standard (50 ng/mL carbamazepine). The samples were centrifuged (3000 rcf, 5 min) and supernatants transferred and diluted 1:1 (supernatant: water) into a new 96-well plate, which was then sealed in preparation for LC/MS/MS analysis.

LC/MS/MS Bioanalysis of Samples from *In Vivo* Assays

In vivo samples were analyzed via electrospray ionization (ESI) on an AB Sciex API-4000 (Foster City, CA) triple-quadrupole instrument that was coupled with Shimadzu LC-10AD pumps (Columbia, MD) and a Leap Technologies CTC PAL auto-sampler (Carrboro, NC). Analytes were separated by gradient elution using a Fortis C18 3.0 x 50 mm, 3 μm column (Fortis Technologies Ltd, Cheshire, UK) thermostated at 40 ºC. HPLC mobile phase A was 0.1% formic acid in water (pH unadjusted), mobile phase B was 0.1% formic acid in acetonitrile (pH unadjusted). The source temperature was set at 500 ºC and mass spectral analyses were performed using multiple reaction monitoring (MRM), with transitions specific for each compound utilizing a Turbo-Ionspray® source in positive ionization mode (5.0 kV spray voltage). The calibration curves were constructed, and linear response was obtained by spiking known amounts of test compound in blank brain homogenate or plasma. All data were analyzed using AB Sciex Analyst software v1.5.1. The final PK parameters were calculated by noncompartmental analysis using Phoenix (version 6.2) (Pharsight Inc., Mountain View, CA).

Supplemental Tables

Table S1. Left-hand aryl substituent VU0134992 SAR. IC_{50} values determined in Tl^+ flux assays from triplicate wells.

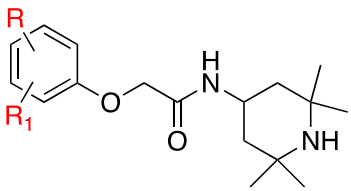

Structure	hKir4.1 IC_{50} (μM)	LCMS
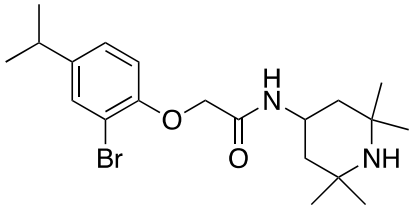	5.2	R.T. 0.757 min, m/z = 411.3 (>98% at 214/254 nM)
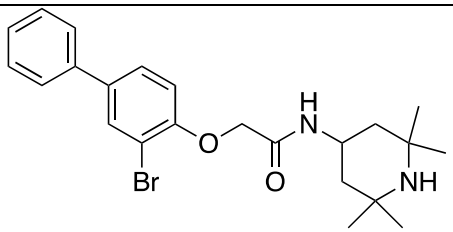	4.8	R.T. 1.012 min, m/z = 445.4 (>98% at 214/254 nM)
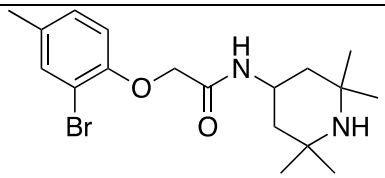	9.9	R.T. 0.711 min, m/z = 383.3 (>98% at 214/254 nM)
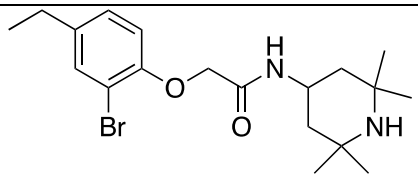	3.0	R.T. 0.721 min, m/z = 397.3 (>98% at 214/254 nM)

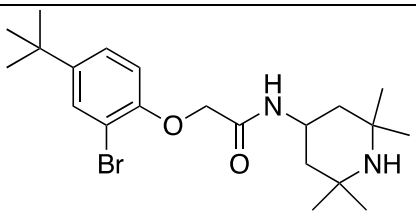	8.0	R.T. 0.894 min, m/z = 425.4 (>98% at 214/254 nM)
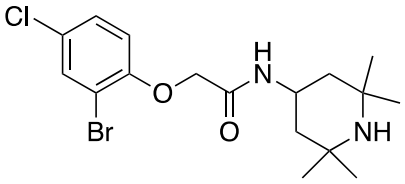	9.7	R.T. 0.799 min, m/z = 403.7 (>98% at 214/254 nM)
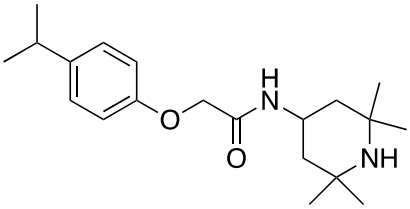	Inactive	R.T. 0.651 min, m/z = 332.4 (>98% at 214/254 nM)
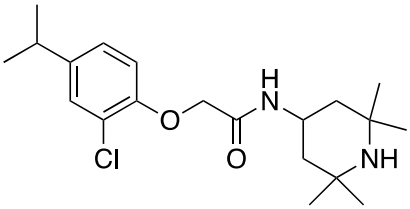	Inactive	R.T. 0.711 min, m/z = 366.93 (>98% at 214/254 nM)
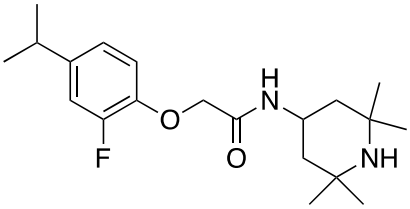	Inactive	R.T. 0.721 min, m/z = 350.4 (>98% at 214/254 nM)
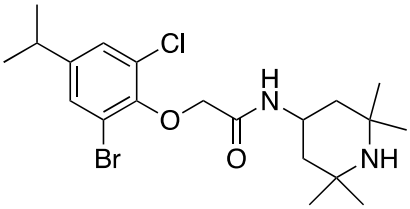	~91	R.T. 0.846 min, m/z = 445.8 (>98% at 214/254 nM)

Table S2. Right-hand piperidine analogs. IC_{50} values determined in Tl^+ flux assays from triplicate wells.

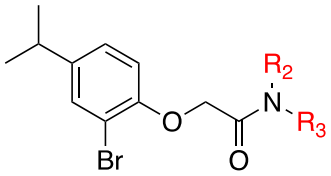

Structure	**hKir4.1 IC_{50} (μM)**	**LCMS**
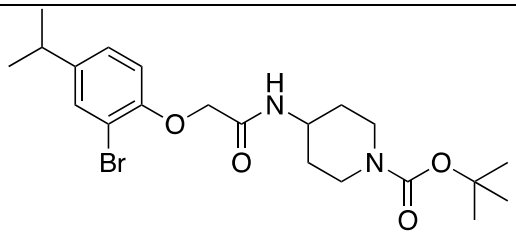	Inactive	R.T. 0.792 min, m/z = 455.3 (>98% at 214/254 nM)
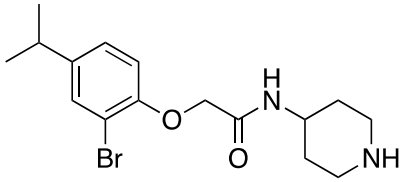	Inactive	R.T. 0.412 min, m/z = 355.2 (>98% at 214/254 nM)
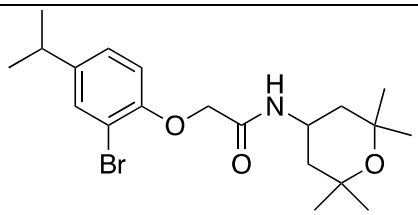	Inactive	R.T. 1.512 min, m/z = 412.3 (>98% at 214/254 nM)
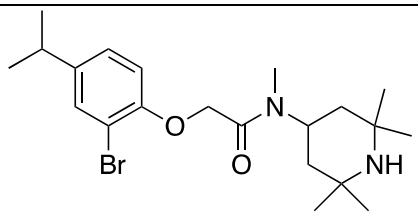	~35	R.T. 0.811 min, m/z = 425.4 (>98% at 214/254 nM)
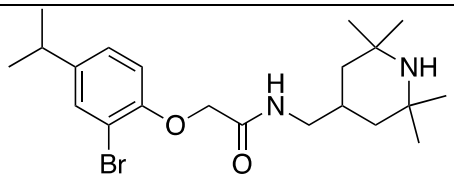	Inactive	R.T. 0.776 min, m/z = 439.4 (>98% at 214/254 nM)

Table S3. Chain-length/spacer SAR. IC_{50} values determined in Tl^+ flux assays from triplicate wells.

Structure	**hKir4.1 IC_{50} (µM)**	**LCMS**
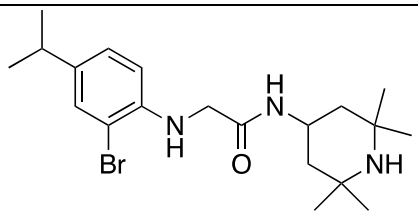	Inactive	R.T. 0.722 min, m/z = 410.4 (>98% at 214/254 nM)
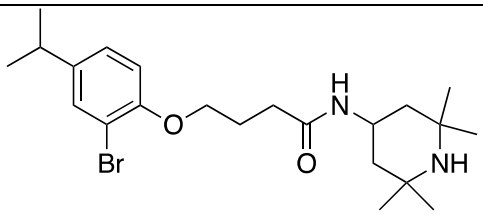	~11	R.T. 0.843 min, m/z = 439.4 (>98% at 214/254 nM)
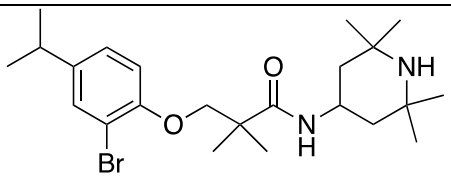	~9	R.T. 0.883 min, m/z = 453.4 (>98% at 214/254 nM)
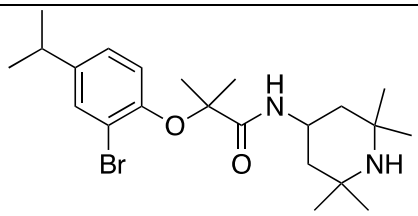	5.2	R.T. 0.757 min, m/z = 411.3 (>98% at 214/254 nM)

Figure S1. Synthetic scheme of VU0134992.

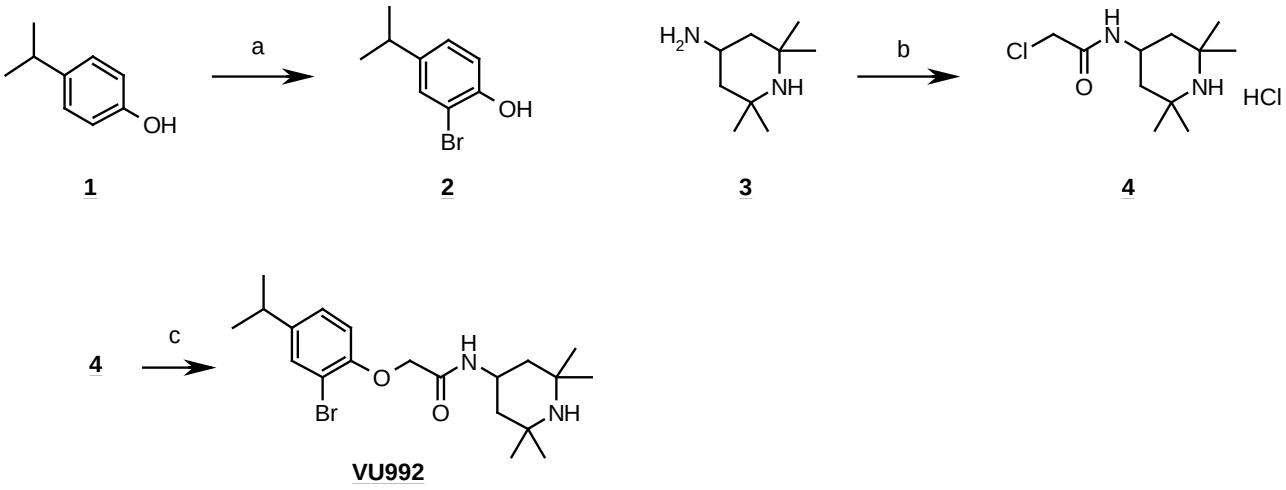

(a) NBS, CH3CN, 0°C, 1.5h, 52%; (b) chloroacetyl chloride, DCM, 0°C, 40min, 97%; (c) **2**, Cs_2CO_3, NaI, DMF, 50°C, 18h 78%.

Figure S2. Synthetic scheme for right-hand piperidine analogs.

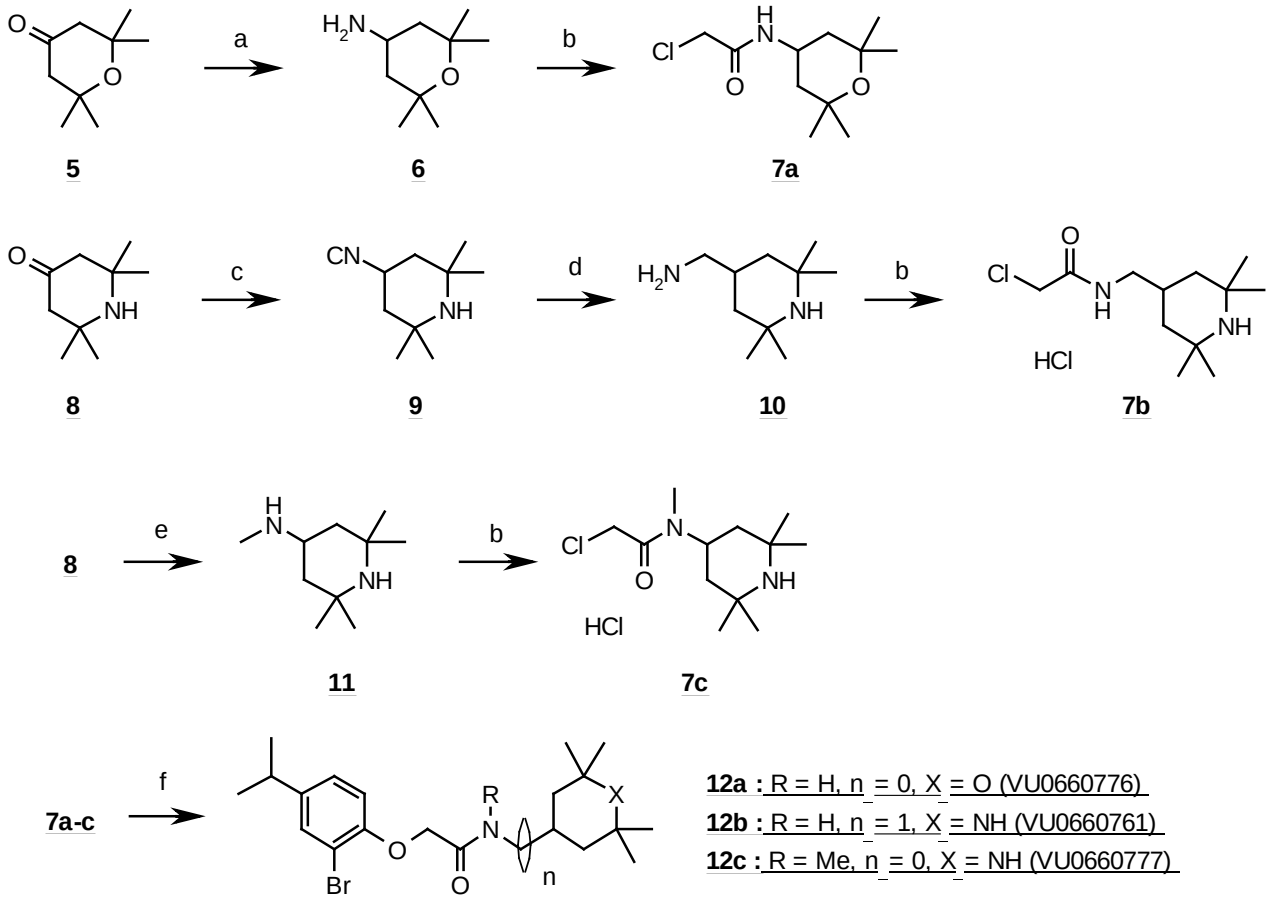

12a : R = H, n = 0, X = O (VU0660776)
12b : R = H, n = 1, X = NH (VU0660761)
12c : R = Me, n = 0, X = NH (VU0660777)

(a) HCO_2NH_4, Pd-C, MeOH/H_2O, r.t., 5h, 44%; (b) chloroacetyl chloride, DCM, 0ºC, 10-20min, (DIPEA for **7a**), 67%-quantitative; (c) TosMIC, *t*-BuOK/*t*-BuOH, DME, 110ºC, 1h, 68%; (d) $LiBH_4$, TMSCl, THF, r.t., 23h, 51%; (e) methylamine hydrochloride, $NaBH(OAc)_3$, TEA, DCM/THF, r.t., 6h, quantitative; (f) 2-bromo-4-iso-propylphenol (**2**), Cs_2CO_3, NaI, DMF, 50 ºC,17-23h, 37-66%.

Figure S3. Synthetic scheme for chain-length/spacer modification.

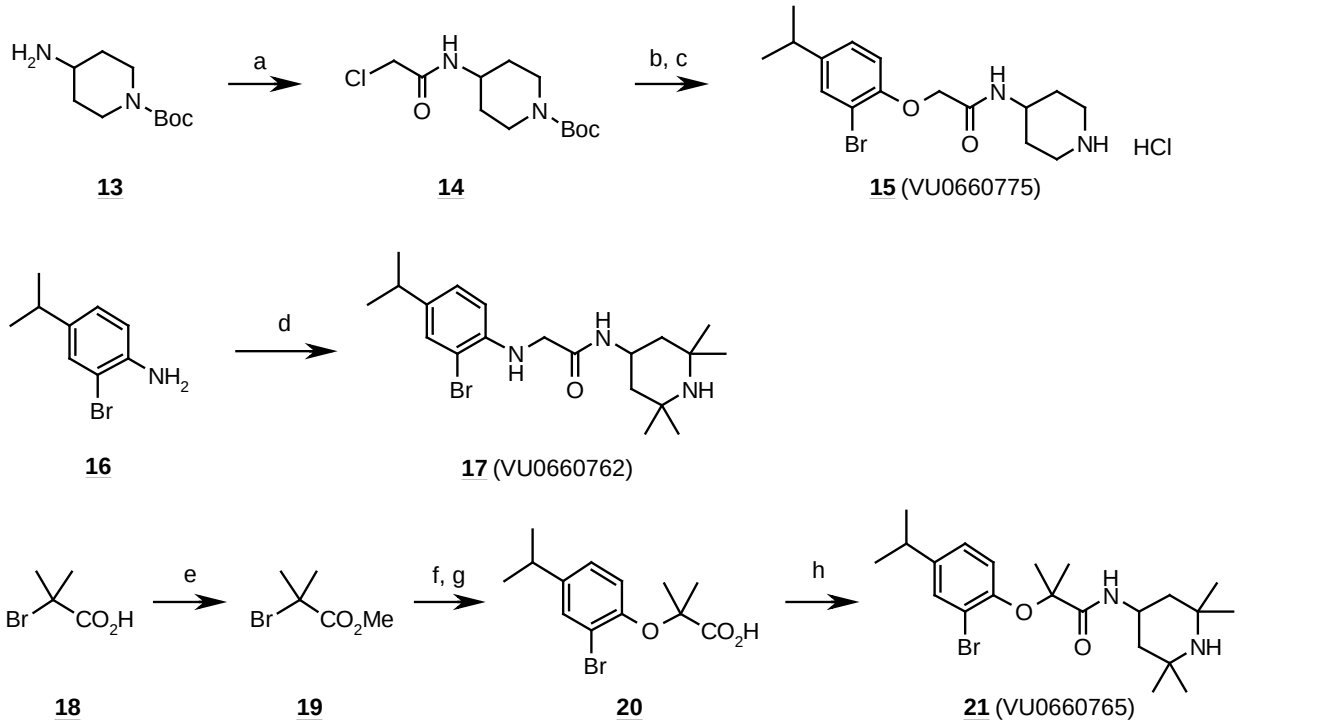

(a) chloroacetyl chloride, DIPEA, DCM, 0°C to r.t., 30min, 89%; (b) 2-bromo-4-iso-propylphenol (**2**), Cs_2CO_3, NaI, DMF, 50°C, 21h, 67%; (c) HCl/1,4-dioxane, 1,4-dioxane, r.t., 16h, 98%; (d) **2**, Cs_2CO_3, NaI, DMF, 90°C, 5.5h, 31%; (e) HCl/MeOH, r.t., 23h, 70%; (f) **2**, Cs_2CO_3, NaI, DMF, microwave irradiation 130°C, 30min, (g) NaOH*aq*, MeOH/THF, 40°C, 5h, 40% in 2 steps; (h) 4-amino-2,2,6,6-tetramethylpiperidine (**3**), HATU, DIPEA, DCM, r.t., 3h, 49%.